Published in final edited form as:

Cell. 2018 July 12; 174(2): 271–284.e14. doi:10.1016/j.cell.2018.05.014.

A metabolite-triggered tuft cell-ILC2 circuit drives small intestinal remodeling

Christoph Schneider[1], **Claire E. O'Leary**[1], **Jakob von Moltke**[1,5], **Hong-Erh Liang**[1], **Qi Yan Ang**[2], **Peter J. Turnbaugh**[2], **Sridhar Radhakrishnan**[3], **Michael Pellizzon**[3], **Averil Ma**[1], and **Richard M. Locksley**[1,2,4,*]

[1]Department of Medicine, University of California San Francisco (UCSF), San Francisco, CA 94143, USA

[2]Department of Microbiology & Immunology, University of California San Francisco (UCSF), San Francisco, CA 94143, USA

[3]Research Diets, Inc., New Brunswick, NJ 08901, USA

[4]Howard Hughes Medical Institute, UCSF

SUMMARY

The small intestinal tuft cell-ILC2 circuit mediates epithelial responses to intestinal helminths and protists by tuft cell chemosensory-like sensing and IL-25-mediated activation of lamina propria ILC2s. Small intestine ILC2s constitutively express the IL-25 receptor, which is negatively regulated by A20 (*Tnfaip3*). A20-deficiency in ILC2s spontaneously triggers the circuit, and, unexpectedly, promotes adaptive small intestinal lengthening and remodeling. Circuit activation occurs upon weaning, and is enabled by dietary polysaccharides that render mice permissive for *Tritrichomonas* colonization, resulting in luminal accumulation of acetate and succinate, metabolites of the protist hydrogenosome. Tuft cells express GPR91, the succinate receptor, and dietary succinate, but not acetate, activates ILC2s via a tuft-, TRPM5-, and IL-25-dependent pathway. Also induced by parasitic helminths, circuit activation and small intestinal remodeling impairs infestation by new helminths, consistent with the phenomenon of concomitant immunity. We describe a metabolic sensing circuit that may have evolved to facilitate mutualistic responses to luminal pathosymbionts.

[*]Corresponding Author/Lead Contact: Dr. Richard M. Locksley, University of California, San Francisco, 513 Parnassus Ave, S-1032B, San Francisco, CA 94143-0795, Telephone: 415-476-5859, richard.locksley@ucsf.edu.
[5]Current position: University of Washington, Seattle, WA 98109, USA.

AUTHOR CONTRIBUTIONS

C.S. conceived the study, designed and performed experiments, analyzed data and wrote the manuscript with R.M.L.. C.E.O. designed and performed experiments, analyzed data and edited the manuscript. J.v.M. generated the *A20*^{fl}RR mice. H.-E.L. assisted with experiments. Q.Y.A. and P.J.T. assisted with energy balance analysis. S.R. and M.P. provided diets. A.M. provided *A20*^{fl} mice. R.M.L. directed the study and wrote the paper with C.S.

DECLARATION OF INTERESTS

The authors declare no competing interests.

In Brief

Succinate produced by mutualistic colonizing protists in the small intestine activates a tuft cell - ILC2 circuit, leading to adaptive remodeling that increases surface area absorption and prevention of other infections.

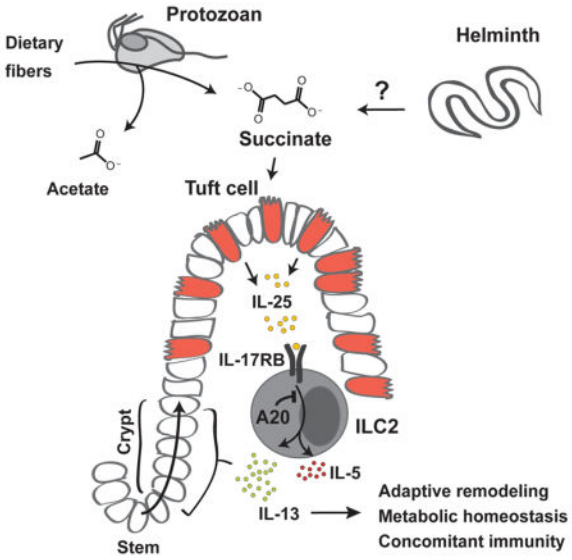

Keywords

Tuft cells; ILC2s; A20; epithelial remodeling; IL-25; TRPM5; eukaryotic pathosymbionts; succinate; succinate receptor; GPR91; hydrogenosome; *Tritrichomonas*; helminths; concomitant immunity

INTRODUCTION

The small intestine is dedicated to nutrient acquisition aided by a complex microbiota and supported by large numbers of immune cells that regulate the balance between tolerance to food, maintenance of the microbiota, and defense against pathogens. Homeostasis at this interface is critical as revealed by increasingly prevalent autoinflammatory bowel diseases (Liu and Stappenbeck, 2016) and food allergies (Tordesillas et al., 2017). Better understanding of the interactions that mediate the dynamic interplay between diet, the microbiota, and the immune cell networks that maintain this barrier is needed to enable strategies to achieve therapeutic reconstruction of this essential mucosal organ.

Recently, several laboratories, including our own, identified a role for epithelial tuft cells in the intestinal response to helminths and protists (Gerbe et al., 2016; Howitt et al., 2016; von Moltke et al., 2016). Long recognized as a constituent of mucosal epithelia in vertebrates, tuft cells remained enigmatic, in part due to the rare frequency of these cells. The apical tuft, which is comprised of microvillus extensions into the lumen, suggested a sensory function, which was supported by the expression of components of the taste receptor signaling cascade in these cells (Sato, 2007). We showed that mucosal tuft cells constitutively express

IL-25, and that these cells increase markedly in small intestinal epithelia after infection with helminths. Activation of tuft cell IL-25 after infection stimulated lamina propria ILC2s to secrete IL-13, which directly biased cell-fate decisions in epithelial stem cell progenitors, resulting in increased goblet and tuft cell frequencies that accompany the 'weep-and sweep' response to worms (von Moltke et al., 2016). An independent manuscript confirmed the role of tuft cells in this cytokine relay using *Pou2f3*-deficient mice, which lack tuft cells (Gerbe et al., 2016). A third group made the important discovery that an unappreciated protozoan pathosymbiont of the genus *Tritrichomonas* also elicited expansion of the tuft cell compartment via this ILC2-mediated epithelial circuit, which depended on TRPM5, a calcium-activated cation channel involved in G protein-coupled taste transduction and highly expressed in tuft cells (Howitt et al., 2016). Recognition of *Tritrichomonas* has uncovered roles for chronic colonization by these organisms in altering not only epithelial cell architecture of the small intestine, but also the 'immunologic tone' of the animals (Chudnovskiy et al., 2016; Escalante et al., 2016). Thus, these eukaryotic pathosymbionts, like certain keystone bacteria (e.g., segmented filamentous bacteria, *Helicobacter* spp.) can impact heterologous infectious or inflammatory processes due to effects on immune or epithelial tissues, or both, with the capacity to mediate tissue protection or pathology under certain conditions. The widespread prevalence of such adapted pathosymbiotic organisms in feral vertebrates, however, suggests a highly evolved mutualism. With this in mind, we undertook a more comprehensive study of factors that impact the small intestinal tuft cell – ILC2 circuit in mice.

RESULTS

Constitutive A20 expression in small intestine ILC2s restrains IL-25-mediated expansion of the tuft cell – ILC2 circuit

Characterization of peripheral ILC2 populations revealed heterogeneity in expression of IL-17RB, which with IL-17RA comprises the heterodimeric IL-25 receptor (Song et al., 2016). IL-17RB transcripts and surface expression were high in small intestinal ILC2s compared to ILC2s from other peripheral tissues, including fat, lung, skin or adjacent gastrointestinal tissues including cecum and colon (Fig. 1A–C). The signaling component of the IL-25 receptor, IL-17RA, and its adapter proteins are negatively regulated by A20 (*Tnfaip3*) (Garg et al., 2013). Indeed, A20 expression was constitutively high in ILC2s from peripheral tissues but not in bone marrow (Fig. 1D), consistent with a role in regulating homeostatic signaling. Further, constitutive high A20 expression was evident in small intestinal ILC2s regardless of age and in germ-free (GF) mice, and was down-regulated after infection with the potent circuit activator, *N. brasiliensis*, consistent with a dynamic role in circuit control (suppl. Fig. 1A).

To delete A20 in ILC2s, we crossed mice with *loxP*-flanked A20 alleles (Tavares et al., 2010) to IL-5 RFP-Cre (Red5) mice (Nussbaum et al., 2013), generating mice that are homozygous A20-floxed with one ($A20^{fl}$R+) or two alleles of Red5 ($A20^{fl}$RR) (suppl. Fig. 1B). A20-deficient ILC2s produced increased cytokines after stimulation *in vitro*, consistent with an inhibitory role for A20 in restraining ILC2 cytokine production (suppl. Fig. 1C). Unexpectedly, $A20^{fl}$RR mice had a marked increase in IL-5-expressing ILC2s in the lamina

propria of small intestine as compared to control mice (Fig. 1E, suppl. Fig. 1D and E); *A20*^{fl}R+ mice were phenotypically comparable to *A20*^{fl}RR mice. Despite deletion of A20 from ILC2s in all tissues analyzed (suppl. Fig. 1B), effects on other tissue ILC2 numbers were much less dramatic; the numbers of ILC2s in the fat were unchanged and lung ILC2s were slightly reduced (suppl. Fig. 1F). The accumulation of ILC2s was accompanied by increased frequencies of DCLK1^{+} tuft cells along the entire small intestine (Fig. 1F and 1G), but not in other parts of the gastrointestinal tract, including the adjacent stomach, cecum and colon (suppl. Fig. 2A). Consistent with prior studies of small intestinal ILC2 activation (Gerbe et al., 2016; Moro et al., 2010; Neill et al., 2010; von Moltke et al., 2016), goblet cells were increased in *A20*^{fl}RR mice but enteroendocrine and Paneth cell numbers remained unchanged (suppl. Fig. 2B and C). Taken together, these data are consistent with spontaneous activation of the small intestinal tuft cell–ILC2 circuit in *A20*^{fl}RR and *A20*^{fl}R+ mice, and reminiscent of what we and others described in the context of intestinal nematode and parabasalid protozoan infection (Gerbe et al., 2016; Howitt et al., 2016; von Moltke et al., 2016).

The feed-forward nature of the tuft cell–ILC2 circuit is driven by IL-25 and IL-13, which are produced by the tuft cells and ILC2s, respectively. To confirm that these cytokines drive circuit activation in *A20*^{fl}RR mice, we crossed *A20*^{fl}RR mice to *Il25*$^{-/-}$ and *Il4ra*$^{-/-}$ mice. Indeed, tuft cell hyperplasia was abrogated in *A20*^{fl}RR mice deficient in IL-25 or IL-4Rα (Fig. 1H and 1I). Further, small intestine IL-5^{+} ILC2s were reduced in *Il25*$^{-/-}$*A20*^{fl}RR and *Il25*$^{-/-}$*A20*^{fl}R+ mice, indicating that IL-25 drives their accumulation in the absence of A20 (Fig. 1I–K). In contrast, elevated numbers of IL-5 and IL-13 reporter-positive ILC2s were present in *Il4ra*$^{-/-}$*A20*^{fl}RR and *Il4ra*$^{-/-}$*A20*^{fl}R+ mice (Fig. 1I–K), confirming the inability of IL-25-producing tuft cells to expand when the epithelial progenitor compartment is unresponsive to IL-13 (von Moltke et al., 2016). Thus, A20 functions as a cell-intrinsic brake on the response of small intestinal ILC2s to IL-25. Despite constitutively high expression of A20 in ILC2s from all peripheral tissues analyzed, the major effects of A20 deletion were restricted to small intestine.

Activation of the tuft cell – ILC2 circuit drives adaptive small intestine remodeling

To assess the effects of small intestine ILC2 activation in *A20*^{fl}RR mice, we quantified the populations of secretory (tuft, goblet, enteroendocrine, Paneth cells) and absorptive enterocytes in the small intestine. As expected, the villus epithelium of *A20*^{fl}RR mice had a significantly increased frequency of secretory cells, with a corresponding decrease in absorptive enterocytes (Fig. 2A and 2B). Together with epithelial alterations, *A20*^{fl}RR mice developed morphological features associated with chronic helminth infection, including crypt hypertrophy and thickening of the surrounding muscularis layer (suppl. Fig. 2D and E) (Garside et al., 2000), consistent with generalized trophic effects restricted to small bowel tissues. To assess whether these changes caused metabolic alterations, we used metabolic cages to monitor parameters of intake, output and energy consumption. To avoid confounding effects introduced by the ablation of IL-5 in homozygous RR mice (Molofsky et al., 2013), we performed these experiments in *A20*^{fl}R+ mice. Unexpectedly, constitutive activation of the tuft cell – ILC2 circuit caused no significant alterations in total oxygen consumption (Fig. 2C) or food intake (Fig. 2D); body weight was slightly but significantly

reduced as compared to control animals (Fig. 2E). Quantification of the caloric density of stool using bomb calorimetry as a measure of non-absorbed energy, however, showed no alterations in *A20*^{fl}R+ mice, consistent with comparable nutrient-extractive capacity of the intestine (Fig. 2F).

The maintenance of energy balance despite marked remodeling of the small intestine led us to consider mechanisms by which animals adapt to constitutive circuit activation. Strikingly, *A20*^{fl}R+ and *A20*^{fl}RR mice showed significant increases in small intestine length, suggesting adaptation driven by dispersal of relatively constant numbers of absorptive enterocytes over the increased surface area (Fig. 2G and 2H). The positive correlation between amplification of the circuit and small intestinal lengthening in *A20*^{fl}R+ and *A20*^{fl}RR mice was further supported by using an independent ILC2-specific A20-deletion strategy with YetCre-13 mice, which contain an IL-13 regulated Cre element (Price et al., 2010), which resulted in comparable phenotypes (suppl. Fig. 3A and 3B). Small intestine lengthening was absent in *A20*^{fl}RR mice crossed with animals deficient in IL-25, IL-4/IL-13 signaling or tuft cells (*Pou2f3*$^{-/-}$), in which circuit amplification is abrogated (Fig. 3A). Small intestine lengthening was also significantly attenuated in *A20*^{fl}RR mice crossed to *Trpm5*-deficient mice, consistent with signaling through a tuft cell sensory pathway (suppl. Fig. 3C).

To test whether amplification of the circuit was sufficient to induce adaptive small intestinal lengthening in wild-type mice, we used recombinant IL-25 to activate ILC2s. Activation of the circuit by 4 daily injections of IL-25, which directly activates small intestinal ILC2s to expand secretory epithelial lineages, increased the caloric density of stool, consistent with acutely decreased absorptive capacity (suppl. Fig. 3D). Chronic administration of IL-25 over four weeks, however, caused tuft cell expansion and significant lengthening of the small intestine as compared to vehicle control (Fig. 3B, suppl. Fig. 3E). Similar adaptation occurred following IL-25 administration to GF mice (Fig. 3C). Adaptive lengthening was absent when IL-25 was given to *Il4ra*$^{-/-}$ mice, but intact in *Pou2f3*$^{-/-}$ mice that lack tuft cells, and demonstrating a dominant effect mediated by stimulation with IL-13 (Fig. 3D and 3E, suppl. Fig. 3F). Hydrodynamic IL-13 overexpression and repeated treatment with rIL-4 complex similarly induced small intestinal lengthening (Fig. 3F and G). Taken together, these data suggest that amplification of the small intestinal tuft cell – ILC2 circuit is necessary and sufficient to induce adaptive remodeling of the small bowel.

Intestinal infections that activate the tuft cell – ILC2 circuit drive adaptive small intestine remodeling

We hypothesized that natural intestinal parasites of mice that activate the intestinal tuft cell – ILC2 circuit, such as *Tritrichomonas* spp. (Howitt et al., 2016) and *H. polygyrus*, would result in similar alterations. We isolated *Tritrichomonas* spp. (here designated *Tritrichomonas*) as confirmed by morphology and detection of 18S rRNA – ITS region on genomic DNA (Fig. 3H, Suppl. Fig. 3G), from cecal contents of colonized animals at UCSF to colonize 3-week old mice from The Jackson Laboratory (JAX) (suppl. Fig. 3H). Two months after colonization, the small bowel of *Tritrichomonas*-colonized mice was significantly longer as compared with non-colonized controls; lengthening did not occur in

colonized *Pou2f3*$^{-/-}$ mice (Fig. 3I). Small intestine length correlated with the frequency of tuft cells and ILC2s (Fig. 3J, suppl. Fig. 3I). To extend these observations, we used another natural mouse parasite, *H. polygyrus*. This nematode induces marked activation of the tuft cell – ILC2 circuit (Howitt et al., 2016; von Moltke et al., 2016); tuft cell hyperplasia is maintained for as long as the luminal worms remain in the small intestine (suppl. Fig. 3J). Again, a significant increase in the length of the small intestine was present at 4 weeks post-infection (Fig. 3K). Thus, chronic amplification of the tuft cell – ILC2 circuit by eukaryotic pathosymbionts promotes small intestinal remodeling associated with adaption to the sustained increases in secretory-absorptive epithelial cell differentiation.

During development, the surface area of the intestine expands to increase absorptive capacity necessary to meet the metabolic requirements for growth, which can be mediated by a process of crypt fission resulting in duplication of stem cell niches required to nucleate additional villi. Crypt hypertrophy was apparent in *A20*^{fl}RR mice (Suppl Fig. 2D) and is a common feature of helminth infections (Garside et al., 2000). To assess whether activation of crypt fission contributes to expansion of the small intestine in mice with an amplified circuit, we performed lineage tracing in Lgr5^{+} intestinal stem cells using CreERT2-mediated induction of the multicolor reporter R26R-Confetti, in which crypt fission events are revealed by the appearance of two or more adjacent labeled clonal crypts bearing the same color. Consistent with previous reports (Snippert et al., 2010), crypt fission rate was low in the small intestine of adult mice (Fig. 3L and M). Mice infected with *H. polygyrus*, in contrast, demonstrated clonal expansion of crypts expressing the same mark, consistent with crypt fission, that was prominent in areas in proximity to the worms (Fig. 3L and M). Crypt fission was less obvious in mice treated with rIL-25, which may reflect additional pathways or the ease of identifying involved areas after worm infection (Fig. 3M). Amphiregulin, a member of the EGF family of growth factors, can promote epithelial proliferation after *Trichuris muris* infection (Zaiss et al., 2006). Although ILC2s can be an important source of amphiregulin (Gury-BenAri et al., 2016; Monticelli et al., 2011), *Areg*-deficent mice showed no diminution in small intestinal lengthening after *H. polygyrus* infection (suppl. Fig. 3K).

Weaning and post-natal differentiation of the tuft cell – ILC2 small intestinal circuit

Because the small intestinal tissue undergoes marked alterations with weaning, we assessed when circuit activation and remodeling occur in *A20*^{fl}RR and control mice. We detected no differences in small intestinal length or tuft cell hyperplasia before (2 wks) and around weaning (4 wks), indicating that amplification of the tuft cell–ILC2 circuit occurs after weaning (Fig. 4A and 4B, Fig. 1). Notably, ILC2s were present, expressed IL-17RB, and became IL-5 reporter-positive as early as p12 (Fig. 4C), and similar to what we previously reported in lung ILC2s (Nussbaum et al., 2013). We noted, however, that levels of IL-5 expression by ILC2s increased significantly between 2 and 5 weeks of age. This increase was abrogated in *Il25*-deficient mice, consistent with ILC2 stimulation by IL-25 after weaning (Fig. 4C and 4D). IL-5 (Red5) expression was largely restricted to CD3^{-}KLRG1^{+}IL-17RB^{+} ILC2s, consistent with a dominant role for innate cells (Suppl. Fig. 4A). Using both IL-25 reporter expression and DCLK1 staining as markers, we found that tuft cells are extremely rare in the first 2 weeks of life, and begin to accumulate around and after weaning (Fig. 4E). IL-13 expression by ILC2s concomitantly increased after weaning

(Fig. 4F), and was accompanied by IL-25-dependent changes in ILC2 marker expression, including decreases in Arg1 and Thy1, and increases in the inhibitory receptor, KLRG1 (suppl Fig. 4B and C). Thus, the basal tuft cell–ILC2 circuit is established post-weaning by a process dependent on IL-25 and negatively regulated by A20 in ILC2s.

Microbiota, diet, and pathosymbionts in priming and activation of the small intestine tuft cell – ILC2 circuit

Weaning is marked by changes from milk to solid food, and is accompanied by substantial alterations in energy expenditure and maturation of the microbiota (Sommer and Backhed, 2013). To assess the overall effects of the microbiota on tuft cell and ILC2 frequency in the small intestine, we analyzed adult GF mice. Using a number of surface markers, we could ascertain little differences in the status of ILC2s from GF mice as indicated by comparable expression of IL-17RB and KLRG1 (Fig. 5A and Suppl. Fig. 5A), and consistent with previous reports (Gury-BenAri et al., 2016); tuft cells were also comparable to those in naïve barrier-maintained mice but were increased in mice from UCSF vivarium that were colonized with *Tritrichomonas* (Fig. 5B). Due to the association with weaning, we explored the effects of milk on the intestinal tuft cell-ILC2 circuit. Feeding adult mice with pasteurized bovine milk as the lone dietary constituent led to reduced IL-13 expression by small intestinal ILC2s (Fig. 5C). Further, *A20*^{fl}RR mice that were kept only on milk diet after weaning had reduced tuft cell hyperplasia and small bowel lengthening (Fig. 5D and 5E). Notably, we detected an increased abundance of *Tritrichomonas* in the cecum following weaning (Fig. 5F), whereas *Tritrichomonas* were significantly depleted by placing colonized mice on a strict milk diet (Suppl. Fig. 5B), but not when milk was provided together with chow diet (Suppl. Fig. 5C), suggesting that dietary change facilitates colonization. Further, depletion of *Tritrichomonas* using metronidazole-treatment of colonized wild-type mice led to reduced IL-13 expression by small intestinal ILC2s (Fig. 5G). Continuous exposure to metronidazole starting from birth prevented tuft cell hyperplasia and small bowel lengthening in exposed and colonized *A20*^{fl}RR mice, whereas a cocktail of broad-spectrum antibiotics that substantially depletes the bacterial microbiota but not *Tritrichomonas* had no effect (Fig. 5H and 5I, Suppl. Fig. 5D). Likewise, tuft cell hyperplasia and small bowel lengthening were significantly reduced in *A20*^{fl}RR mice that were raised free of *Tritrichomonas* (Fig. 5H and 5I). IL-13 expression was induced in ILC2s of *A20*^{fl}R+ mice upon colonization with protists and preceded the accumulation of tuft cells and intestinal lengthening (Fig. 5J and 5K, suppl. Fig. 5E and 5F). Thus, the switch from milk to solid food corresponds with developmental priming of the tuft cell–ILC2 circuit mediated by widespread eukaryotic pathosymbionts, such as *Tritrichomonas* and helminths, but not bacteria, in concordance with prior reports (Gerbe et al., 2016; Howitt et al., 2016; von Moltke et al., 2016).

Parabasalid protozoa are common endobiotic symbionts of the intestinal tract in wood-digesting invertebrates such as termites, where the protists help to digest complex plant polysacharride fibers; persistent colonization across the social colony is actively maintained through anal-oral transmission by proctodeal trophallaxis (Brune, 2014). To address whether *Tritrichomonas* in coprophagic mice utilize complex dietary fibers, which are a major dietary constituent of feral and laboratory rodents, we fed mice isocaloric fiber-manipulated

diets (Table S1). Notably, *Tritrichomonas* were heavily depleted when dietary fibers were absent or when cellulose was the sole fiber (Fig. 5L, suppl. Fig. 5G). In contrast, *Tritrichomonas* colonization became re-established when the oligofructan inulin was the sole dietary fiber (Fig. 5L, suppl. Fig. 5G). The fermentable fiber requirement for *Tritrichomonas* colonization and circuit activation was accompanied by abrogation of tuft cell hyperplasia and lengthening when *A20*^{fl}R+ mice were fed cellulose diet, but substantial reconstitution on inulin diet (Fig. 5M, suppl. Fig. 5H).

Products of *Tritrichomonas* metabolism activate the tuft cell – ILC2 circuit

Fermentation of dietary fibers by the microbiota results in the generation of short-chain fatty acids (SCFAs) and other carboxylic acids, which impact many aspects of host physiology, including metabolism and immunity (Koh et al., 2016). Indeed, we detected increased cecal acetate in SPF mice colonized with *Tritrichomonas* (suppl. Fig. 6A). To assess whether these prevalent protists directly contribute to the production of these fermentation products, we monocolonized GF mice with *Tritrichomonas*. Notably, we found increased cecal acetate and succinate levels in GF mice colonized with *Tritrichomonas* (Fig. 6A and 6B), consistent with fermentative pyruvate oxidation in the protist hydrogenosomes (Muller et al., 2012). Because we noted high expression of G-protein coupled receptors for SCFAs (*Ffar3*) and succinate (*Sucnr1*) in tuft cells (Fig. 6C), we hypothesized that *Tritrichomonas*-derived metabolic end products might be sensed directly by tuft cells. Strikingly, succinate in drinking water induced potent proliferation and IL-13 expression in ILC2s (Fig. 6D–F), which was independent of bacterial microbiota as indicated using GF mice (suppl. Fig. 6B). In contrast, acetate or a mix of acetate, butyrate and propionate did not activate ILC2s (Fig. 6E and 6F). Notably, we detected no *Sucnr1* expression in ILC2s (suppl. Fig. 6C). Further, succinate-mediated ILC2 activation required the presence of tuft cells and IL-25, and was significantly reduced in the absence of TRPM5 (Fig. 6E and 6F), demonstrating a crucial function in sensing luminal succinate and consistent with the role of the tuft cell – TRPM5 – IL-25 axis in detecting luminal pathosymbionts (Gerbe et al., 2016; Howitt et al., 2016; von Moltke et al., 2016) and with TRPM5-redundant pathways (Dutta Banik et al., 2018). The effects of luminal succinate were limited to ILC2s of the small intestine (suppl. Fig. 6D–F), consistent with highest expression of *Sucnr1* by small intestinal tuft cells (suppl. Fig. 6G). Succinate-induced circuit activation resulted in increased tuft cell frequencies similar to colonization with *Tritrichomonas* (Fig. 6G), and was restricted by A20 in ILC2s, as indicated by pronounced tuft cell hyperplasia in succinate-treated (*Tritrichomonas*-free) *A20*^{fl}R+ mice that was IL-25-dependent (Fig. 6H). Importantly, succinate alone was sufficient to induce small intestinal lengthening in *A20*^{fl}R+ mice (Fig. 6I). Overall, our results identify the first luminal metabolite capable of activating the tuft cell – ILC2 circuit, and support the chemosensory role that was assigned to tuft cells decades ago.

Activation of the tuft cell – ILC2 circuit contributes to concomitant immunity

The interdependence of development, diet and eukaryotic pathosymbionts in these lines of uncolonized, colonized (*Tritrichomonas*) and infected (*H. polygyrus*) mice allowed us to establish a hierarchical relationship between these luminal states and activation of the small intestinal ILC2-tuft cell circuit (Fig. 7A). To assess the stability of the small intestinal response, we cleared *Tritrichomonas* from the intestines of colonized adult *A20*^{fl}R+ mice.

After two weeks, tuft cell frequencies had essentially normalized to levels that remained only slightly higher than those found in uncolonized control mice (Fig. 7B). Despite this, the numbers of small intestinal IL-5 reporter-positive ILC2s remained increased, even though their expression of IL-13 (as a dynamic marker of activation (Liang et al., 2011)) had become attenuated (suppl. Fig. 7A and 7B). Notably, the difference in small intestinal length was maintained, suggesting that adaptive remodeling was sustained and had become discordant from tuft cell hyperplasia (Fig. 7C). To confirm the generalizable nature of these findings, we determined that wild-type mice previously treated with recombinant IL-25 or infected with *H. polygyrus*, continued to have significant increases in small intestinal length up to 2 months later (Fig. 7D), at a time when the tuft cell composition of the small intestine had almost normalized (suppl. Fig. 7C).

We considered the hypothesis that epithelial re-wiring mediated by activation of the tuft cell – ILC2 circuit might contribute to concomitant immunity, the mechanism by which helminth-infected animals become resistant to new infection despite the inability to reject the primary infection (Smithers and Terry, 1969). Indeed, constitutive activation of the tuft cell – ILC2 circuit in *Tritrichomonas*-colonized *A20*^{fl}RR mice rendered animals resistant to infection by both *N. brasiliensis* and *H. polygyrus* (Fig. 7E–G), and was mediated by *Tritrichomonas* and dependent on IL-25 and tuft cells (Fig. 7G). Circuit activation in *Rag1*$^{-/-}$ mice by pre-treatment with IL-25 sigificantly reduced fecundity of *N. brasiliensis* suggesting that innate components are sufficient to mediate this response, and consistent with prior reports (Suppl. Fig. 7D) (Fallon et al., 2006). We also noted less robust infection with *N. brasiliensis* in mice previously infected and cleared of a heterologous parasites, *H. polygyrus*, in accordance with prior observations (Guo et al., 2015).

DISCUSSION

Our studies illuminate important findings relevant to small intestinal biology. First, although we and others called attention to expression of IL-25 by tuft cells in mucosal epithelia, we now link this with constitutive expression of the IL-25 receptor on small intestine ILC2s, and in contrast to ILC2s in other peripheral organs. This dedicated role for IL-25 in dynamically regulating small bowel homeostasis was further supported by the marked effect of ILC2-specific A20 deletion in sensitizing the small intestinal circuit with minimal effects on other tissue ILC2s. Second, our studies reveal a novel tripartite interplay between this circuit, diet and microbiota, which involved the protist-derived fermentative end-product succinate, which alone activates the circuit leading to adaptive intestinal remodeling, thus revealing a molecular signal promoting luminal detection. Third, an unsuspected component of the host response to chronic circuit activation consisted of small intestine lengthening and remodeling by a process associated with maintenance of systemic energy balance suggesting a conserved physiologic response that likely evolved to sustain host metabolic needs in the face of chronic parasite infestations, which are widespread among feral vertebrates. Lastly, the small intestinal physiologic changes, including tuft cell hyperplasia and small intestinal dynamic lengthening, although induced by viable luminal parasites themselves, impaired further intestinal infection by similar or even heterologous organisms, revealing an evolved host-parasite interaction that served to limit further colonization. Such détente is consistent with the phenomenon of concomitant immunity discovered almost fifty years ago (Smithers

and Terry, 1969), and suggest that remodeling of the intestinal niche by IL-25 plays a key role in enabling a mutualistic state facilitating metabolic homeostasis in the host and a reproductive niche for the pathosymbiont.

Intriguingly, small intestine ILC2s constitutively express the IL-25 receptor, even in GF mice, revealing a dedicated role for these cells in setting the secretory-absorptive tone of the small intestine. In this way, intestinal ILC2s, which seed tissues during fetal development (Bando et al., 2015), resemble fetal-derived tissue macrophages (Mass et al., 2016) in their capacity to integrate into tissues and acquire organ-specific ability to sense anticipatory signals, like tuft cell IL-25, that appear postnatally. The activation of ILC2s in response to luminal eukaryotic pathosymbionts revealed heterogeneity in expression of cytokines like IL-5 and IL-13, and markers like Arginase 1 and Thy1 (Bando et al., 2013; Spits et al., 2013), consistent with observations using single-cell approaches (Gury-BenAri et al., 2016). IL-25 is a member of a family of IL-17 cytokines that occupy a key position at the interface of epithelia, innate immune cells and the microbiota (Song et al., 2016). These cytokines have deep evolutionary roots as assessed by sequence and functional analyses that indicate predominant expression by epithelia and immune cells at barriers that interface with microbes (Buckley et al., 2017; Han et al., 2015); dysregulation of these circuits can cause immunopathology (Amatya et al., 2017). Emerging roles for IL-17 family members in neural networks (Choi et al., 2016), including in nematodes (Chen et al., 2017), are consistent with broader roles in homeostasis. Amplification of the circuit in mice using exogenous IL-25 alone increased small intestinal length, as noted above, that was dependent on IL-4Rα signaling and bypassed the need for tuft cells, as shown in *Pou2f3*$^{-/-}$ mice. Intriguingly, crypt fission rates were increased in proximity to *H. polygyrus*, suggesting that small intestinal surface expansion might be mediated in part by multiplication of existing crypts. Notably, adaptive surface growth following small bowel resection is a well-described phenomenon in humans regulated by multiple hormones and growth factors (Warner, 2016), and roles for circuit amplification, perhaps involving additional tuft cell signals (Middelhoff et al., 2017) and nerve-epithelial interactions (Hayakawa et al., 2017), merit further study.

Intestinal immunity is influenced by complex interactions between dietary components and microbiota (Belkaid and Harrison, 2017). Although ILC2s occupy small intestine at birth, tuft cells appeared coincident with weaning. In our mouse facility, ILC2 activation and tuft cell expansion increased further in animals colonized by vertically-transmitted *Tritrichomonas*, corroborating observations from other SPF facilities (Chudnovskiy et al., 2016; Escalante et al., 2016; Howitt et al., 2016). These organisms are members of the ‘eukaryome’, including protists, fungi and helminths, that are widely prevalent in the vertebrate intestine of asymptomatic humans and animals (Lukes et al., 2015). The parabasalids represent an abundant group of flagellated endobiotic symbionts, commensals and parasites that commonly inhabit the digestive tract. *Tritrichomonas* has also been shown to promote IL-18-dependent Th1 and Th17 immunity in the colon under different conditions (Chudnovskiy et al., 2016; Escalante et al., 2016). Whether these observations reflect species-specific effects and/or tropism-related bias in immunomodulation remains unclear and requires further phylogenetic analysis of protists derived from various research facilities, which might reveal unappreciated diversity as indicated by early descriptions of enteric protozoa in wild rodents (Ring, 1959). We demonstrated a key role for dietary fiber in

enabling *Tritrichomonas* colonization, which could be met by inulin but not cellulose, suggesting similar dietary functions as shown in termite parabasalid symbionts, which are critical for digestion of complex carbohydrates like lignocellulose (Brune, 2014). The capacity of *Tritrichomonas* to degrade recalcitrant complex polysaccharides is consistent with genomic replication of glycolytic enzymes (Barratt et al., 2016) and fermentative metabolism culminating in metabolic end-products of the mitochrondria-like hydrogenosomes, including acetate, succinate and hydrogen (Muller et al., 2012). Notably, other eukaryotic pathosymbionts, including helminths, share similar metabolic pathways (Muller et al., 2012). Important roles for dietary fiber and SCFA in vertebrate physiology are increasingly apparent, and unappreciated roles for prevalent parabasilid organisms in these metabolic interactions with host and bacteria will be of much interest (Koh et al., 2016).

We demonstrate that tuft cells express the succinate receptor, SUCNR1 (GPR91), at high levels as compared to other intestinal epithelia. Succinate, an end-product of *Tritrichomonas* metabolism, potently activated the circuit in a POU2F3-, IL-25- and TRPM5-dependent manner, consistent with a metabolite-triggered sensory role for tuft cells. Krebs cycle intermediates like succinate provide exquisite barometers of cellular energetic stability; small accumulations drive inflammatory programs in macrophages fueling the generation of mitochondrial reactive oxygen intermediates (Mills et al., 2016). Due to export and detection by GPR91, succinate has local and systemic signaling capacity with roles in multiple tissues, including kidney, heart, liver, retina and white adipose tissue, and has been implicated in tissue hypertrophy (Gilissen et al., 2016). Our results suggest that succinate sensing has evolved to detect certain pathosymbionts, such as *Tritrichomonas*, but also succinate-producing bacteria, which, depending on the context, might also be present. Tuft cell-mediated detection of succinate, a potential signal of hypoxic stress and injury (Gilissen et al., 2016), in order to activate ILC2s is consistent with the function of the latter in integrating tissue-derived homeostatic signals (von Moltke and Locksley, 2014), and might enable therapeutic strategies for restoring intestinal adaptation and regeneration in response to inflammation.

In addition to supporting metabolic homeostasis, circuit activation altered the intestinal niche such that further infections were attenuated. This state, termed concomitant immunity, was conceptualized in studies of schistosomiasis in monkeys 50 years ago (Smithers and Terry, 1969), and has been explained largely by adaptive immunity, antigenic variation amongst parasite stages, and Tregs. Our studies suggest that intestinal remodeling mediated by activation of the tuft cell – ILC2 circuit contributes to concomitant immunity by altering the intestinal niche, consistent with aspects of innate tissue memory, or ‘training’ (Netea and van der Meer, 2017). As such, effects on intestinal remodeling mediated by these eukaryotic pathosymbionts extend the concept of colonization resistance (Buffie and Pamer, 2013). Indeed, protective effects have been described across kingdoms as suggested by resistance of *Tritrichomonas*–colonized mice to *Salmonella* infection (Chudnovskiy et al., 2016). Our findings emphasize the deep evolutionary relationships of the ‘eukaryome’, including protozoa and helminths, in sustaining the resilience of the small intestine during development and dietary fluctuations, and suggest key roles for tuft cells, succinate and IL-25 in achieving this mutualistic state. We speculate that harnessing such organisms may

enhance the capacity for extraction of nutrients from complex carbohydrates, and could contribute to the remarkable adaptability of the omnivorous gut.

STAR METHODS

CONTACT FOR REAGENT AND RESOURCE SHARING

Further information and requests for resources and reagents should be directed to and will be fulfilled by the Lead Contact, Richard M. Locksley (richard.locksley@ucsf.edu).

EXPERIMENTAL MODEL AND SUBJECT DETAILS

Mice—A20-floxed mice (*Tnfaip3*^{tm2Ama}) (Tavares et al., 2010) were provided by A. Ma and crossed with *Il5*^{R} mice (Nussbaum et al., 2013) that express a dimer red fluorescent protein (tdTomato) linked by an internal ribosomal entry site (IRES) to a Cre element under the control of the *Il5* locus resulting in conditional deletion of *A20* in ILC2s (*A20*^{fl}R). B6.*Trpm5*−/− (B6.129P2-*Trpm5*^{tm1Dgen}/J, 005848), Lgr5EGFP-CreERT2 (B6.129P2-*Lgr5*$^{tm1(cre/ERT2)Cle}$/J; 008875) and wild-type (C57BL/6J; 000664) mice were purchased from Jackson Laboratories. R26R-Confetti (B6.129P2-*Gt(ROSA)26Sor*$^{tm1(CAG-Brainbow2.1)Cle}$/J) were provided by O. Klein. B6.*Areg*−/− (*Areg*^{tm1Dle}) were provided by M. Conti. Arginase-1 reporter Yarg (B6.129S4-*Arg1*^{tm1Lky}/J), B6.*Il25*−/−, IL-13 reporter Smart13 (B6.129S4(C)-*Il13*$^{tm2.1Lky}$/J), Il13-cre (C.129S4(B6)-*Il13*$^{tm1(YFP/cre)Lky}$/J), B6.*Il4ra*−/− and IL-25 reporter (*Il25*^{F25}) mice were obtained or generated as described (Van Dyken et al., 2014) (Liang et al., 2011) (von Moltke et al., 2016). B6.*Pou2f3*−/− (C57BL/6N-*Pou2f3*$^{tm1.1(KOMP)Vlcg}$) were provided by M. Anderson. Mice were maintained in the University of California San Francisco specific pathogen–free animal facility or UCSF Gnotobiotic Core Facility in accordance with the guidelines established by the Institutional Animal Care and Use Committee and Laboratory Animal Resource Center. SPF animals were housed in individually ventilated cage units that are changed every three weeks for maintenance cages and every other week for breeding cages; cage bottoms are covered with autoclaved bedding and nesting material for enrichment. Mice were fed irradiated food (PicoLab Mouse Diet 20, 5058M) and drink from autoclaved bottles or automatic watering system. All animals were manipulated using standard procedures including filtered air exchange stations, chlorine-based disinfection of gloves and work surfaces within manipulations with animals; personnel protection equipment (PPE) (disposable gowns, gloves, head caps, and shoe covers) is required to enter the facility. Mice aged 6–14 weeks were used for all experiments, except for specific long-term experiments. Experiments were carried out using age and gender matched groups. Unless otherwise noted, all strains of mice that were housed within the UCSF vivarium were positive for *Tritrichomonas* and was confirmed for experimental mice in cecal content by visual inspection or qPCR. Standard animal manipulation procedures prevented contamination of *Tritrichomonas*-free strains that were housed in the same room. To establish *Tritrichomonas*-free colonies mice were treated with drinking water supplemented with 2.5 g/l metronidazole and 1% sucrose for 2–3 weeks. WT C57BL/6J were originally obtained from Jackson Laboratories and maintained in the UCSF vivarium following colonization with *Tritrichomonas* or uncolonized.

METHOD DETAILS

Mouse infection and treatment—Mice were infected subcutaneously with 500 *N. brasiliensis* L3 or by oral gavage with 200 *H. polygyrus* L3, and were killed at the indicated time points to collect tissues for staining or to count intestinal worm burden, as described (von Moltke et al., 2016). To clear *H. polygyrus* mice were treated with a single dose of 2 mg pyrantel pamoate (Columbia Laboratories) by oral gavage. IL-25 (R&D Systems) was administered intraperitoneally in doses of 500 ng on four consecutive days during the first week followed by 3 doses per week for the subsequent 3 weeks. All injections were given in 200 µl. For the milk diet, whole cow's milk (Costco Wholesale) was the only source of food and/or drink as indicated, and was replaced daily. Custom diets were formulated based on an open standard diet (D11112201; Research Diets, Inc.) and contained no fiber (D11112229), 10 % cellulose (D17030102) or 10% inulin (D11112226) (Table S1). For antibiotic-treatment experiments, mice received drinking water supplemented with ampicillin, metronidazole, neomycin (1 mg/ml each), and vancomycin (0.5 mg/ml) in 1% sucrose, or metronidazole (2.5 mg/ml) in 1% sucrose as indicated. For SCFA and succinate treatments, succinic acid (100 mM), sodium acetate (100 mM), or a SCFA mix (67.5 mM sodium acetate, 40 mM sodium butyrate, 25.9 mM sodium propionate) were provided in the drinking water and changed weekly. For hydrodynamic gene delivery, mouse IL-13 coding sequence was cloned into pLIVE in vivo expression vector (Mirus Bio). Plasmid DNA was purified using EndoFree Plasmid Mega Kit (Qiagen). Mice received hydrodynamic tail-vein injections of 1 µg plasmid DNA in a volume equal to 10% body weight (0.1 ml/g) within +/− 5 s. As a control, a hIgG1 expression vector was injected. rIL-4 complexes were generated by incubating 2 µg animal-free recombinant mouse IL-4 (PeproTech) with 10 µg InVivoPlus anti-mouse IL4 antibody (clone 11B11, Bio X Cell) for 30 min at room temperature, and administered i.p. as described for rIL-25. For GF experiments, fecal pellets were regularly analyzed for microbial contamination using PCR and standard culture techniques.

Intestine length—Immediately after euthanasia, the small intestine was cut distal to the stomach, carefully pulled out of the abdomen and detached from mesenteric tissue. After cutting proximal to the cecum, the small intestine length was measured by hanging vertically alongside a measuring tape.

Fixed tissue preparation and staining—For immunohistochemistry, tissues were flushed with PBS and fixed in 4% paraformaldehyde for 2–3 h at 4 °C followed by PBS wash and overnight incubation in 30% (w/v) sucrose. Intestines were coiled into a 'Swiss roll', tissues were embedded in Optimal Cutting Temperature Compound (Tissue-Tek) and stored at −80 °C before sectioning (8 µm) on a Cryostat (Leica). Staining was performed in Tris/NaCl blocking buffer (0.1 M Tris-HCl, 0.15 M NaCl, 5 µg/ml blocking reagent (Perkin Elmer), pH 7.5) as follows: 1 h 5% goat serum, 1 h primary antibody, 40 min secondary antibody, 5 min DAPI (Roche). For RFP and DCLK1 co-labelling experiments, slides were stained for RFP as described above, excluding the DAPI step. DCLK staining was as follows: 30 min rabbit IgG (Abcam, ab27472), 1 h anti-DCLK1-AF488, and 5 min DAPI. See Key Resources Table for a list of antibodies used in this study.

For goblet cell staining, intestinal tissues were fixed for 3 h in 10% buffered formalin (Fisher Scientific) at 4 °C before coiling into a 'Swiss roll' and returning to formalin. After 24 h, tissues were moved to 70% ethanol for storage. Tissue processing, paraffin embedding, and sectioning were performed by the UCSF Mouse Pathology Core. Periodic acid Schiff (PAS) and Alcian blue staining were performed as follows: cleared with xylenes (Fisher Scientific), rehydrated, 30 min in Alcian blue (Thermo Scientific), 5 min in periodic acid (Thermo Scientific), 15 min in Schiff reagent (Thermo Scientific), dehydrated, and mounted. Brightfield and fluorescent images were acquired with an AxioCam HR camera on an AxioImagerM2 upright microscope (Zeiss).

Single-cell tissue preparation—Lungs were perfused through the heart with cold PBS and harvested. Single-cell suspensions were prepared using a gentleMACS tissue dissociator (Miltenyi Biotec), running program lung_01 followed by incubation for 35 min at 37° C in RPMI-1640 containing 50 μg/ml Liberase TM (Roche) and 25 μg/ml DNase I (Roche), and then running gentleMACS program lung_02. The tissue was passed through 70-μm nylon filters, washed, and subjected to red blood cell lysis (PharmLyse; BD) before final suspension in FACS buffer (PBS, 3% FCS, 0.05% NaN_3). Perigonadal visceral adipose tissue (VAT) was harvested and finely minced with scissors, followed by incubation for 40 min at 37° C in RPMI-1640 containing 100 μg/ml Liberase TM (Roche) and 50 μg/ml DNase I (Roche). The tissue was passed through 100-μm nylon filters, washed, and subjected to red blood cell lysis (PharmLyse; BD) before final suspension in FACS buffer. For lamina propria preparations, a 6 cm piece of small intestine was harvested, flushed with PBS, opened, and thoroughly cleaned with PBS.

Intestines were incubated for 20 min in 20 ml HBSS (Ca^{2+}/Mg^{2+} free) supplemented with 2% fetal calf serum (FCS), 10 mM HEPES (UCSF Cell Culture Facility) and 5 mM DTT. Supernatants were discarded and intestines were incubated for 15 min in 10 ml HBSS (Ca^{2+}/Mg^{2+} free) supplemented with 2% fetal calf serum (FCS), 10 mM HEPES (UCSF Cell Culture Facility) and 5 mM EDTA solution. This step was repeated twice using fresh solution. Next, intestines were incubated for 10 min in 20 ml HBSS (with Ca^{2+}/Mg^{2+}) supplemented with 3% FCS and 10 mM HEPES. After incubation, intestines were gently vortexed, cut into small pieces and incubated for 30 min in 5 ml HBSS (with Ca^{2+}/Mg^{2+}) supplemented with 3% FCS, 10 mM HEPES, 100 μg/ml Liberase TM (Roche) and 30 μg/ml DNase I (Roche). All the incubations were performed with gentle rocking at 37 °C. After digest, intestines were mechanically dissociated in GentleMACS C tubes (Miltenyi Biotec) using program m_intestine_01, passed through a 100 μm filter, and washed. The resulting cell pellet was resuspended in 5 ml 40% Percoll (Sigma-Aldrich), underlaid with 5 ml 90% Percoll and centrifuged at 2000 r.p.m. for 20 min at 20 °C. The 40/90 interphase of the Percoll gradient was harvested, washed, and stained for flow cytometry. EDTA washes were pooled and stained for epithelial cell analysis by flow cytometry.

Flow cytometry—Single-cell suspensions were incubated with Fc Block (Bio X Cell, 2.4G2) followed by staining with antibodies to surface markers. Lineage (Lin) cocktail included (CD3, CD4, CD5, CD8α, CD11b, CD11c, CD19, CD49b, NK-1.1, F4/80, TER-119, Gr-1, FcεRIα, TCR γ/δ). Exclusion of DAPI (4′,6-diamidine-2′-phenylindole

dihydrochloride; Roche) identified live cells, which were enumerated with flow cytometric counting beads (CountBright Absolute; Life Technologies). Cells were kept on ice throughout staining procedure. See Supplementary Table 1 for a list of antibodies used in this study.

For intracellular DCLK1 staining, single-cell epithelial suspensions were incubated with Violet Live/Dead fixable stain (Life Technologies), fixed in 4% paraformaldehyde (Electron Microscopy Sciences) for 5–10 min, washed and stained in permeabilization buffer (ThermoFisher, 00-8333-56) with rabbit anti-DCLK1 (Abcam; ab31704; 1:4000) in perm/wash and rat anti-EpCAM-PerCP-Cy5.5 (Biolegend; G8.8; 1:300) for 20 min, followed by F(ab′)2 goat anti-rabbit IgG-Alexa Fluor 488 (Life Technologies; 1:4000) for 15 min. For intracellular staining of transcription factors, the FoxP3/Transcription Factor Staining Buffer Set (eBiosciences) was used according to manufacturer's instructions.

Samples were analyzed on a LSRFortessa Dual (BD Biosciences) with five lasers (355 nm, 405 nm, 488 nm, 561 nm and 640 nm). Samples were FSC-A/SSC-A gated to exclude debris, FSC-H/FSC-A gated to select single cells, and gated to exclude DAPI+ dead cells. Data were analyzed with FlowJo 9 (Treestar).

Tuft and secretory cell quantification—Single-cell epithelial suspension were prepared as described, analyzed by flow cytometry and the frequency of tuft cells was calculated as number of DCLK1+ cells/total number of EPCAM+CD45− cells. Because the viability of epithelial cells was found to be very low when prepared from *A20*^{fl}R mice or worm-infected intestines, a shorter protocol was used when such samples were analyzed: 6 cm pieces of small intestine were harvested, flushed with PBS, opened, and thoroughly cleaned with PBS. Next tissues were cut into 0.5 cm pieces, gently vortexed in 20 ml PBS and incubated with gentle rocking for 15 min at 37 °C in 5 ml PBS (Ca^{2+}/Mg^{2+} free) supplemented with 5% FCS, 10 mM HEPES, 1mM DTT and 4 mM EDTA. Samples were vortexed, centrifuged, resuspended in FACS buffer, passed through 100-μm nylon filters, washed, and stained. Alternatively, tuft cell frequency was quantified in frozen tissue sections by staining for DCLK1 as described earlier. A 4 × 4 grid of images was collected at ×100 magnification and the number of tuft cells was quantified on more than 25 villi using AxioVision software (Zeiss). Tuft cell numbers were calculated as DCLK1+ cells per mm villus length. For secretory cell quantification, tissue sections were stained for MUC2, LYZ1, CHRA, DCLK1 and EpCAM as described above. The number of cells positive for MUC2, LYZ1, CHRA or DCLK1 was assessed for 100 adjacent EpCAM+ cells per villus for 10 villi per sample.

Crypt fission—Crypt fission in the small intestine was assessed as described previously (Snippert et al., 2014). Briefly, Lgr5EGFP-CreERT2;R26R-Confetti mice were treated intraperitoneally with 4 mg of tamoxifen (Sigma-Aldrich) in 200 μl corn oil (Sigma-Aldrich) three times over the course of a week during which they were also kept on a tamoxifen diet (TD.130858; Envigo). 4 weeks after tamoxifen treatment the mice were infected with 200 *H. polygyrus* L3 and were killed on d28 post-infection to harvest small intestine. For whole-mount imaging, 1.5 cm pieces were cut open longitudinally, villi were scraped off using a coverslip and tissues were flushed with PBS before fixation in 4% paraformaldehyde at

room temperature for 60 minutes. Next, parts were washed in PBS, transferred to a microscope slide with crypt bottoms oriented to the top and mounted in vectashield (Vector Laboratories). Confocal images were acquired using a Leica SP5 Inverted Confocal microscope. Images were processed using Imaris (Bitplane), ImageJ and Photoshop. At least 200 Lgr5EGFP+ crypts per sample were counted, of which the percentage of R26R-Confetti + clones in singlet, doublet and triplet or more clusters was quantified.

Quantitative RT–PCR—Single-cell epithelial suspensions were isolated, stained as described earlier and sorted using a MoFlo XDP (Beckman Coulter). RNA was isolated using the Micro Plus RNeasy kit (Qiagen) and reverse transcribed using the SuperScript Vilo Master Mix (Life Technologies). The resulting cDNA was used as template for quantitative PCR (qPCR) with the Power SYBR Green reagent on a StepOnePlus cycler (Applied Biosystems). Transcripts were normalized to *Rps17* (40S ribosomal protein S17) expression and relative expression shown as $2^{-\Delta Ct}$. Primer sequences (see also Key Resources Table): *Rps17*, 5′-CGCCATTATCCCCAGCAAG-3′, 5′-TGTCGGGATCCACCTCAATG-3′; *A20*, 5′-ACAGGACTTTGCTACGACAC-3′, 5′-CTGAGGATGTTGCTGAGGAC-3′; *Il17rb*, 5′-GGCTGCCTAAACCACGTAATG-3′, 5′-CCCGTTGAATGAGAATCGTGT-3′; *Tritrichomonas*, 5′-AGAGGAAGGAGAAGTCGTAACAAGG-3′, 5′-CTCGTGTAAGAAGCCAAGACATCC-3′; Eubacteria 16S, 5′-ACTCCTACGGGAGGCAGCAGT-3′, 5′-ATTACCGCGGCTGCTGGC-3′; *Sucnr1* (PrimerBank 14161704a1), 5′-TCTTGTGAGAATTGGTTGGCAA-3′, 5′-CATCTCCATAGGTCCCCTTATCA-3′; *Ffar2* (PrimerBank 22122727a1), 5′-CTTGATCCTCACGGCCTACAT-3′, 5′-CCAGGGTCAGATTAAGCAGGAG-3′; *Ffar3* (PrimerBank 142345193c1), 5′-CTTCTTTCTTGGCAATTACTGGC-3′, 5′-CCGAAATGGTCAGGTTTAGCAA-3′; *Hcar2* (PrimerBank 13507640a1), 5′-CTGGAGGTTCGGAGGCATC-3′, 5′-TCGCCATTTTTGGTCATCATGT-3′.

***Tritrichomonas* quantification—**Genomic DNA was isolated from cecal content using QIamp Fast DNA Stool mini kit (Qiagen) according to the manufacturers instructions. *Tritrichomonas* gDNA was quantified by qPCR and normalized to Eubacteria 16S rRNA gene using the method $2^{-\Delta Ct\,(Tritrichomonas\text{-}16S)}$.

***Tritrichomonas* purification—**For *Tritrichomonas* isolation, the cecal content colonized mice was harvested, washed 3 times with 50 ml PBS, during which it was filtered twice through a 100 μm cell strainer and centrifuged at 1000 rpm for 10 min. Motile protists were enumerated using a hemocytometer. For GF colonization, PBS containing 100 mg/ml streptomycin, 100 U/ml penicillin and 50 μg/ml Vancomycin was used for all washing steps and protists were double sorted using a MoFlo XDP (Beckman Coulter) with a a 90 μm nozzle, spun down and resuspended in PBS at 100 Mio/ml. Culture of *Tritrichomonas* was performed as recently described (Chudnovskiy et al., 2016) with the following modifications. Briefly, cecal extract was generated by diluting cecal content isolated from *Tritrichomonas*-free mice with 25 volumes of PBS (1 g content per 25 ml PBS), stirred at 4 °C for 6 hr, spun down at 3500 rpm for 10 min and the supernatant was filtered through 100 μm strainer. The filtered cecal extract was used to resuspend the TrichoselTM broth (Becton Dickinson) according to the manufacturer's protocol and titrated to pH 7 with

NaOH. The medium was autoclaved prior to be supplemented with filter-sterilized 10% heat-inactivated horse serum (Gibco) and antibiotics including 100 μg/ml streptomycin, 100 U/ml penicillin (UCSF Cell Culture Facility), 50 μg/ml Vancomycin (Gold Biotechnology), 10 μg/ml Ciprofloxacin (Sigma), 20 μg/ml gentamicin and 0.5 μg/ml amphotericin B (ThermoFisher). Protists were inoculated at 2 Mio/ml in pre-equilibrated growth media and cultured in an anaerobic chamber (Coy) at 37 °C for 3 days on a MACSmix™ Tube Rotator (Miltenyi) at maximal speed. Then, the suspension was diluted in 50 ml PBS, centrifuged at 1000 rpm for 10 min and resuspended in PBS. Primary GF recipient mice received filter-sterilized drinking water supplemented with ampicillin, streptomycin, neomycin, bacitracin (1 mg/ml each), 125 μg/ml ciprofloxacin, 100 μg/ml ceftazimidine, 150 μg/ml gentamicin, 200 μg/ml amphotericin B (all from Sigma) and 0.5 mg/ml vancomycin (Gold Biotechnology) in 1% sucrose, which was started 3 days prior to inoculation with 2 Mio protists. 3 weeks later, absence of bacteria and fungi was confirmed using PCR and standard culture techniques, cecal content was harvested and diluted in PBS. 2 Mio protists were gavaged into 5–6 week old GF mice, which were again tested repeatedly for microbial contamination and analyzed 6 weeks later.

In vitro cell cultures—Sorted cells were cultured (37 °C, 5% CO_2) at 3000–5000 cells/well in high-glucose DMEM supplemented as follows: 4.5 g/L glucose, 0.584 g/L l-glutamine, 3.7 g/L $NaHCO_3$, 1× nonessential amino acids, 1× minimal essential vitamins, 0.116 g/L l-arginine HCl, 0.036 g/L l-asparagine, 0.006 g/L folic acid, 10% FBS, 100 mg/ml streptomycin, 100 U/ml penicillin, 10 mM Hepes, 1 mM Na pyruvate, 100 μM 2-ME, and 2 mM l-glutamine. Cells were stimulated for 3 days with 10 ng/ml IL-7 (R&D Systems) or 10 ng/ml IL-33 (R&D Systems), as indicated. At harvest, cell-free culture supernatants were collected for protein analysis, while cells were resuspended and stained for flow cytometric analysis.

Cytokine quantification—Cytokine levels in cell culture supernatant were measured using Cytokine Bead Array Flex Sets (BD) according to the manufacturer's protocol and data was analyzed using Flow Cytometric Analysis Program (FCAP) Array software (BD).

Metabolic assays—Whole-animal metabolic analysis was performed using CLAMS cages (Comprehensive Laboratory Animals Monitoring System) per the manufacturer's instructions (Columbus Instruments). In brief, animals were singly housed and measurements were taken every 12 min for 4 days, including oxygen consumption, carbon dioxide output, food consumption, water consumption, and three unique measures of movement. Respiratory exchange ratio and heat were calculated asVCO2/VO2 (RER) and VO2(3.815 + 1.232 × RER; heat), respectively. Heat, VO2, and VCO2 were all normalized to effective body mass Vxx = Vxx/[(weight(g)/mass unit)]0.75, per the manufacturer's recommendations. To measure animal adiposity and lean mass, MRI was performed using an EchoMRI according to the manufacturer's instructions (Echo Medical Systems LTD).

Fecal energy content—Fecal samples were collected and lyophilized to obtain dried mass. 100–200 mg of dried stool was pressed into a pellet using a pellet press. Gross energy content was measured using a isoperibol oxygen bomb calorimeter with a semimicro oxygen

bomb (Models 6200 and 1109, respectively, from Parr Instrument Co.). The calorimeter energy equivalent factor was determined using benzoic acid standards.

Measurement of short-chain fatty acid and succinate concentrations—In order to measure cecal lumenal short chain fatty acids, a sample of cecal content was weighed and stored at −80 °C until analyzed. Samples and serially diluted standards were acidified using 6N HCl (1 volume of HCl to 5 volume of diluted sample) in the presence of 400 μM acetic acid-d4 and valeric acid (internal standards), then extracted with equal volume of ether. Solid samples (cecal content, fecal pellet) were lysed using a Qiagen TissueLyser II. The ether fraction was derivatized by MTBSTFA (1 to 10 volume of ether fraction) at room temperature for greater than 24 hrs, and used for GCMS for detection. Samples were run on Agilent Technologies 5977A GC/MSD system and short chain fatty acids were normalized to wet weight. For the succinate quantification in the cecal content, snap frozen samples were processed using a colorimetric succinate assay kit (Abcam, ab204718) according to the manufacturer's instructions, including deproteinization and decolorization.

QUANTIFICATION AND STATISTICAL ANALYSIS

All experiments were performed using randomly assigned mice without investigator blinding. All data points and n values reflect biological replicates. No data were excluded. Where noted in the figures, statistical significance was calculated using two-tailed non-parametric Mann-Whitney *U* test was used for the comparison between two experimental groups or one-way ANOVA for multiple comparisons. Experimental groups included a minimum of three biological replicates. Intragroup variation was not assessed. All statistical analysis was performed using Prism 6 (GraphPad Software). Figures display means ± s.e.m. as indicated. No statistical methods were used to predetermine sample size.

Supplementary Material

Refer to Web version on PubMed Central for supplementary material.

Acknowledgments

We thank Z. Wang, M. Ji and M. Consengco for technical expertise; members of the Locksley lab for discussions; O. Klein and M. Anderson for manuscript comments; C.J. Guo and M.A. Fischbach for assistance with SCFA measurements; J. Turnbaugh and UCSF Gnotobiotic Core Facility for GF mice; the UCSF BIDC for assistance with confocal microscopy; and the Mouse Metabolism Core at the UCSF DRC and NORC for assistance with metabolic experiments. This work was supported by grants AI26918, AI30663, HL128903, and HL122593 from the NIH, HHMI, and the SABRE Center at the UCSF. C.S. is supported by fellowships from the Swiss National Science Foundation (P2EZP3_162266; P300PA_171591). P.J.T. is a Nadia's Gift Foundation Innovator supported by the Damon Runyon Cancer Research Foundation (DRR-42-16), the UCSF Program for Breakthrough Biomedical Research, and the Searle Scholars Program.

References

Amatya N, Garg AV, Gaffen SL. IL-17 Signaling: The Yin and the Yang. Trends Immunol. 2017; 38:310–322. [PubMed: 28254169]

Bando JK, Liang HE, Locksley RM. Identification and distribution of developing innate lymphoid cells in the fetal mouse intestine. Nat Immunol. 2015; 16:153–160. [PubMed: 25501629]

Bando JK, Nussbaum JC, Liang HE, Locksley RM. Type 2 innate lymphoid cells constitutively express arginase-I in the naive and inflamed lung. J Leukoc Biol. 2013; 94:877–884. [PubMed: 23924659]

Barratt J, Gough R, Stark D, Ellis J. Bulky Trichomonad Genomes: Encoding a Swiss Army Knife. Trends Parasitol. 2016; 32:783–797. [PubMed: 27312283]

Belkaid Y, Harrison OJ. Homeostatic Immunity and the Microbiota. Immunity. 2017; 46:562–576. [PubMed: 28423337]

Brune A. Symbiotic digestion of lignocellulose in termite guts. Nat Rev Microbiol. 2014; 12:168–180. [PubMed: 24487819]

Buckley KM, Ho ECH, Hibino T, Schrankel CS, Schuh NW, Wang G, Rast JP. IL17 factors are early regulators in the gut epithelium during inflammatory response to Vibrio in the sea urchin larva. Elife. 2017; 6:860.

Buffie CG, Pamer EG. Microbiota-mediated colonization resistance against intestinal pathogens. Nat Rev Immunol. 2013; 13:790–801. [PubMed: 24096337]

Chen C, Itakura E, Nelson GM, Sheng M, Laurent P, Fenk LA, Butcher RA, Hegde RS, de Bono M. IL-17 is a neuromodulator of Caenorhabditis elegans sensory responses. Nature. 2017; 542:43–48. [PubMed: 28099418]

Choi GB, Yim YS, Wong H, Kim S, Kim H, Kim SV, Hoeffer CA, Littman DR, Huh JR. The maternal interleukin-17a pathway in mice promotes autism-like phenotypes in offspring. Science. 2016; 351:933–939. [PubMed: 26822608]

Chudnovskiy A, Mortha A, Kana V, Kennard A, Ramirez JD, Rahman A, Remark R, Mogno I, Ng R, Gnjatic S, et al. Host-Protozoan Interactions Protect from Mucosal Infections through Activation of the Inflammasome. Cell. 2016; 167:444–456. e414. [PubMed: 27716507]

Dutta Banik D, Martin LE, Freichel M, Torregrossa AM, Medler KF. TRPM4 and TRPM5 are both required for normal signaling in taste receptor cells. Proc Natl Acad Sci U S A. 2018; 115:E772–E781. [PubMed: 29311301]

Escalante NK, Lemire P, Cruz Tleugabulova M, Prescott D, Mortha A, Streutker CJ, Girardin SE, Philpott DJ, Mallevaey T. The common mouse protozoa Tritrichomonas muris alters mucosal T cell homeostasis and colitis susceptibility. J Exp Med. 2016; 213:2841–2850. [PubMed: 27836928]

Fallon PG, Ballantyne SJ, Mangan NE, Barlow JL, Dasvarma A, Hewett DR, McIlgorm A, Jolin HE, McKenzie AN. Identification of an interleukin (IL)-25-dependent cell population that provides IL-4, IL-5, and IL-13 at the onset of helminth expulsion. J Exp Med. 2006; 203:1105–1116. [PubMed: 16606668]

Garg AV, Ahmed M, Vallejo AN, Ma A, Gaffen SL. The deubiquitinase A20 mediates feedback inhibition of interleukin-17 receptor signaling. Sci Signal. 2013; 6:ra44. [PubMed: 23737552]

Garside P, Kennedy MW, Wakelin D, Lawrence CE. Immunopathology of intestinal helminth infection. Parasite Immunol. 2000; 22:605–612. [PubMed: 11123752]

Gerbe F, Sidot E, Smyth DJ, Ohmoto M, Matsumoto I, Dardalhon V, Cesses P, Garnier L, Pouzolles M, Brulin B, et al. Intestinal epithelial tuft cells initiate type 2 mucosal immunity to helminth parasites. Nature. 2016; 529:226–230. [PubMed: 26762460]

Gilissen J, Jouret F, Pirotte B, Hanson J. Insight into SUCNR1 (GPR91) structure and function. Pharmacol Ther. 2016; 159:56–65. [PubMed: 26808164]

Guo L, Huang Y, Chen X, Hu-Li J, Urban JF Jr, Paul WE. Innate immunological function of TH2 cells in vivo. Nat Immunol. 2015; 16:1051–1059. [PubMed: 26322482]

Gury-BenAri M, Thaiss CA, Serafini N, Winter DR, Giladi A, Lara-Astiaso D, Levy M, Salame TM, Weiner A, David E, et al. The Spectrum and Regulatory Landscape of Intestinal Innate Lymphoid Cells Are Shaped by the Microbiome. Cell. 2016; 166:1231–1246. e1213. [PubMed: 27545347]

Han Q, Das S, Hirano M, Holland SJ, McCurley N, Guo P, Rosenberg CS, Boehm T, Cooper MD. Characterization of Lamprey IL-17 Family Members and Their Receptors. J Immunol. 2015; 195:5440–5451. [PubMed: 26491201]

Hayakawa Y, Sakitani K, Konishi M, Asfaha S, Niikura R, Tomita H, Renz BW, et al. Nerve Growth Factor Promotes Gastric Tumorigenesis through Aberrant Cholinergic Signaling. Cancer Cell. 2017; 31:21–34. [PubMed: 27989802]

Howitt MR, Lavoie S, Michaud M, Blum AM, Tran SV, Weinstock JV, Gallini CA, Redding K, Margolskee RF, Osborne LC, et al. Tuft cells, taste-chemosensory cells, orchestrate parasite type 2 immunity in the gut. Science. 2016; 351:1329–1333. [PubMed: 26847546]

Koh A, De Vadder F, Kovatcheva-Datchary P, Backhed F. From Dietary Fiber to Host Physiology: Short-Chain Fatty Acids as Key Bacterial Metabolites. Cell. 2016; 165:1332–1345. [PubMed: 27259147]

Liang HE, Reinhardt RL, Bando JK, Sullivan BM, Ho IC, Locksley RM. Divergent expression patterns of IL-4 and IL-13 define unique functions in allergic immunity. Nat Immunol. 2011; 13:58–66. [PubMed: 22138715]

Liu TC, Stappenbeck TS. Genetics and Pathogenesis of Inflammatory Bowel Disease. Annu Rev Pathol. 2016; 11:127–148. [PubMed: 26907531]

Lukes J, Stensvold CR, Jirku-Pomajbikova K, Wegener Parfrey L. Are Human Intestinal Eukaryotes Beneficial or Commensals? PLoS Pathog. 2015; 11:e1005039. [PubMed: 26270819]

Mass E, Ballesteros I, Farlik M, Halbritter F, Gunther P, Crozet L, Jacome-Galarza CE, Handler K, Klughammer J, Kobayashi Y, et al. Specification of tissue-resident macrophages during organogenesis. Science. 2016; 353:aaf4238–aaf4238. [PubMed: 27492475]

Middelhoff M, Westphalen CB, Hayakawa Y, Yan KS, Gershon MD, Wang TC, Quante M. Dclk1-expressing tuft cells: critical modulators of the intestinal niche? Am J Physiol Gastrointest Liver Physiol. 2017; 313:G285–G299. [PubMed: 28684459]

Mills EL, Kelly B, Logan A, Costa ASH, Varma M, Bryant CE, Tourlomousis P, Dabritz JHM, Gottlieb E, Latorre I, et al. Succinate Dehydrogenase Supports Metabolic Repurposing of Mitochondria to Drive Inflammatory Macrophages. Cell. 2016; 167:457–470. e413. [PubMed: 27667687]

Molofsky AB, Nussbaum JC, Liang HE, Van Dyken SJ, Cheng LE, Mohapatra A, Chawla A, Locksley RM. Innate lymphoid type 2 cells sustain visceral adipose tissue eosinophils and alternatively activated macrophages. J Exp Med. 2013; 210:535–549. [PubMed: 23420878]

Monticelli LA, Sonnenberg GF, Abt MC, Alenghat T, Ziegler CG, Doering TA, Angelosanto JM, Laidlaw BJ, Yang CY, Sathaliyawala T, et al. Innate lymphoid cells promote lung-tissue homeostasis after infection with influenza virus. Nat Immunol. 2011; 12:1045–1054. [PubMed: 21946417]

Moro K, Yamada T, Tanabe M, Takeuchi T, Ikawa T, Kawamoto H, Furusawa J, Ohtani M, Fujii H, Koyasu S. Innate production of T(H)2 cytokines by adipose tissue-associated c-Kit(+)Sca-1(+) lymphoid cells. Nature. 2010; 463:540–544. [PubMed: 20023630]

Muller M, Mentel M, van Hellemond JJ, Henze K, Woehle C, Gould SB, Yu RY, van der Giezen M, Tielens AG, Martin WF. Biochemistry and evolution of anaerobic energy metabolism in eukaryotes. Microbiol Mol Biol Rev. 2012; 76:444–495. [PubMed: 22688819]

Neill DR, Wong SH, Bellosi A, Flynn RJ, Daly M, Langford TK, Bucks C, Kane CM, Fallon PG, Pannell R, et al. Nuocytes represent a new innate effector leukocyte that mediates type-2 immunity. Nature. 2010; 464:1367–1370. [PubMed: 20200518]

Netea MG, van der Meer JW. Trained Immunity: An Ancient Way of Remembering. Cell Host Microbe. 2017; 21:297–300. [PubMed: 28279335]

Nussbaum JC, Van Dyken SJ, von Moltke J, Cheng LE, Mohapatra A, Molofsky AB, Thornton EE, Krummel MF, Chawla A, Liang HE, et al. Type 2 innate lymphoid cells control eosinophil homeostasis. Nature. 2013; 502:245–248. [PubMed: 24037376]

Price AE, Liang HE, Sullivan BM, Reinhardt RL, Eisley CJ, Erle DJ, Locksley RM. Systemically dispersed innate IL-13-expressing cells in type 2 immunity. Proc Natl Acad Sci U S A. 2010; 107:11489–11494. [PubMed: 20534524]

Ring M. Studies on the Parasitic Protozoa of Wild Mice from Berkshire with a Description of a New Species of Trichomonas. Proceedings of the Zoological Society of London. 1959; 132:381–401.

Sato A. Tuft cells. Anat Sci Int. 2007; 82:187–199. [PubMed: 18062147]

Smithers SR, Terry RJ. Immunity in schistosomiasis. Ann N Y Acad Sci. 1969; 160:826–840. [PubMed: 4981050]

Snippert HJ, Schepers AG, van Es JH, Simons BD, Clevers H. Biased competition between Lgr5 intestinal stem cells driven by oncogenic mutation induces clonal expansion. EMBO Rep. 2014; 15:62–69. [PubMed: 24355609]

Snippert HJ, van der Flier LG, Sato T, van Es JH, van den Born M, Kroon-Veenboer C, Barker N, Klein AM, van Rheenen J, Simons BD, et al. Intestinal crypt homeostasis results from neutral competition between symmetrically dividing Lgr5 stem cells. Cell. 2010; 143:134–144. [PubMed: 20887898]

Sommer F, Backhed F. The gut microbiota--masters of host development and physiology. Nat Rev Microbiol. 2013; 11:227–238. [PubMed: 23435359]

Song X, He X, Li X, Qian Y. The roles and functional mechanisms of interleukin-17 family cytokines in mucosal immunity. Cell Mol Immunol. 2016; 13:418–431. [PubMed: 27018218]

Spits H, Artis D, Colonna M, Diefenbach A, Di Santo JP, Eberl G, Koyasu S, Locksley RM, McKenzie AN, Mebius RE, et al. Innate lymphoid cells--a proposal for uniform nomenclature. Nat Rev Immunol. 2013; 13:145–149. [PubMed: 23348417]

Tavares RM, Turer EE, Liu CL, Advincula R, Scapini P, Rhee L, Barrera J, Lowell CA, Utz PJ, Malynn BA, et al. The ubiquitin modifying enzyme A20 restricts B cell survival and prevents autoimmunity. Immunity. 2010; 33:181–191. [PubMed: 20705491]

Tordesillas L, Berin MC, Sampson HA. Immunology of Food Allergy. Immunity. 2017; 47:32–50. [PubMed: 28723552]

Van Dyken SJ, Mohapatra A, Nussbaum JC, Molofsky AB, Thornton EE, Ziegler SF, McKenzie AN, Krummel MF, Liang HE, Locksley RM. Chitin activates parallel immune modules that direct distinct inflammatory responses via innate lymphoid type 2 and gammadelta T cells. Immunity. 2014; 40:414–424. [PubMed: 24631157]

von Moltke J, Ji M, Liang HE, Locksley RM. Tuft-cell-derived IL-25 regulates an intestinal ILC2-epithelial response circuit. Nature. 2016; 529:221–225. [PubMed: 26675736]

von Moltke J, Locksley RM. I-L-C-2 it: type 2 immunity and group 2 innate lymphoid cells in homeostasis. Curr Opin Immunol. 2014; 31:58–65. [PubMed: 25458996]

Warner BW. The Pathogenesis of Resection-Associated Intestinal Adaptation. Cell Mol Gastroenterol Hepatol. 2016; 2:429–438. [PubMed: 27722191]

Zaiss DM, Yang L, Shah PR, Kobie JJ, Urban JF, Mosmann TR. Amphiregulin, a TH2 cytokine enhancing resistance to nematodes. Science. 2006; 314:1746. [PubMed: 17170297]

Highlights

- Tuft cell IL-25 and IL-25R+ ILC2s drive A20-regulated small bowel adaptability
- Circuit activation and small bowel hypertrophy maintain systemic energy balance
- Succinate, a *Tritrichomonas* metabolite, triggers tuft cell chemosensation and IL-25
- Circuit activation impedes new helminth infection and enables concomitant immunity

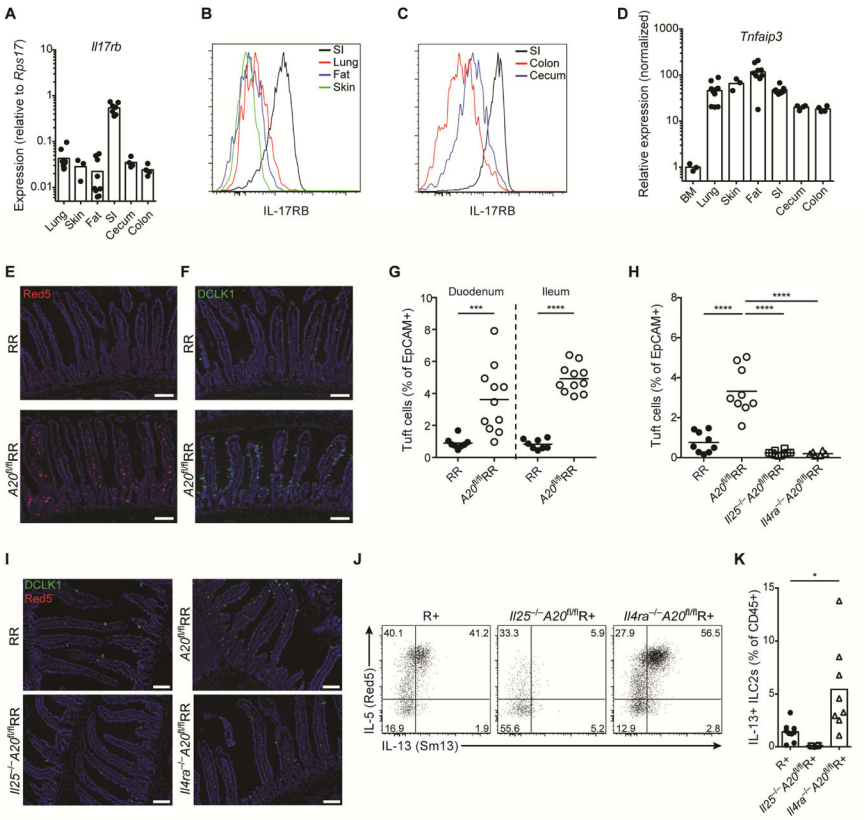

Figure 1. Constitutive high A20 expression in small intestine ILC2s restrains IL-25-mediated expansion of the tuft cell – ILC2 circuit

(A–C) IL-17RB expression measured by qPCR (A) or flow cytometry (B and C) in ILC2s from indicated tissues. (D) A20 expression measured by qPCR in sorted ILC2s from indicated tissues, normalized to BM. (E and F) Presence of ILC2s (E) and tuft cells (F) in the small intestine (SI) of RR and *A20*^{fl}RR mice, visualized by expression of IL-5 (Red5 reporter) in red (E) and DCLK1 in green (F); DAPI in blue. (G and H) Quantification of tuft cells in SI by flow cytometry. (G) Tuft cell frequencies in proximal and distal SI of RR and *A20*^{fl}RR mice. (H) Percentages of tuft cells in SI of RR, *A20*^{fl}RR mice, *Il25*$^{-/-}$*A20*^{fl}RR mice and *Il4ra*$^{-/-}$*A20*^{fl}RR mice. (I) Presence of ILC2s and tuft cells in SI as in (E and F) from mice as in (H). (J) Flow cytometry analysis of IL-13 (Sm13 reporter) and IL-5 (Red5 reporter) expression by ILC2s gated on CD45+Lin-IL-17RB+KLRG1+ cells isolated from the SI of R+, *Il25*$^{-/-}$*A20*^{fl}R+ and *Il4ra*$^{-/-}$*A20*^{fl}R+ mice. (K) Percentages of IL-13+ ILC2s among CD45+ lamina propria cells as in (J). Data pooled from multiple independent experiments (A–D, G, H, K) or from one experiment representative of at least two independent experiments (E, F, I, J). Scale bars; 100 μm. *p < 0.05, ***p < 0.001, ****p < 0.0001; ns, not significant by Mann-Whitney *U* or one-way ANOVA.

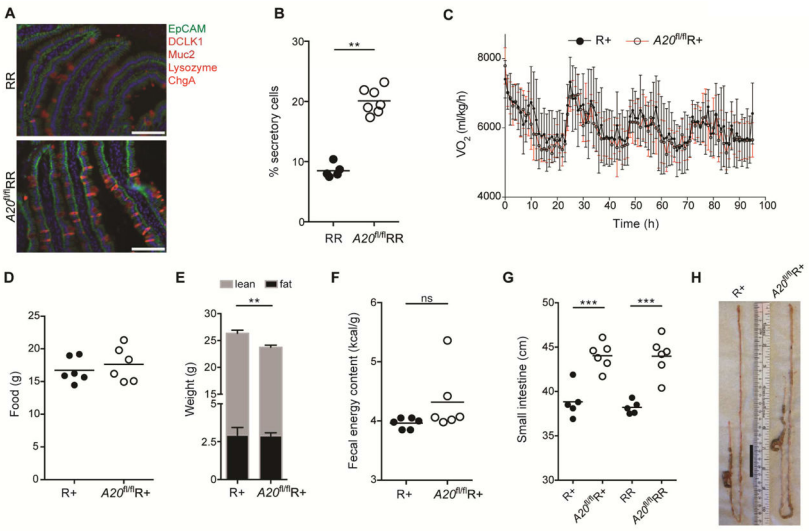

Figure 2. Energy balance in *A20*^{fl}RR mice is associated with an elongated small intestine

(A, B) Quantification of secretory cells by immunofluorescence analysis of RR and *A20*^{fl}RR mice; secretory cell types in red identified by staining for Muc2 (goblet cells), DCLK1 (tuft cells), ChromograninA (ChgA, enteroendocrine cells) and lysozyme (Paneth cells), EpCAM in green, DAPI in blue. (C–F) Metabolic parameters of R+ and *A20*^{fl}R+ mice. (C) Oxygen consumption rate measured using CLAMS cages. (D) Food intake during a 4 day period. (E) Lean and adipose weight determined by EchoMRI. (F) Fecal energy content measured using bomb calorimetry. (G and H) Small intestine (SI) length (G) and representative image (H) of 8–12 week old R+, *A20*^{fl}R+, RR and *A20*^{fl}RR mice. The black bar indicates difference in SI length. Scale bars; 100 μm. Data from one experiment representative of at least three independent experiments (A–E, G, H) or from one experiment (F). (E, mean and s.e.m., n = 10–11). **p < 0.01, ***p < 0.001, ****p < 0.0001; ns, not significant by Mann-Whitney *U* or one-way ANOVA.

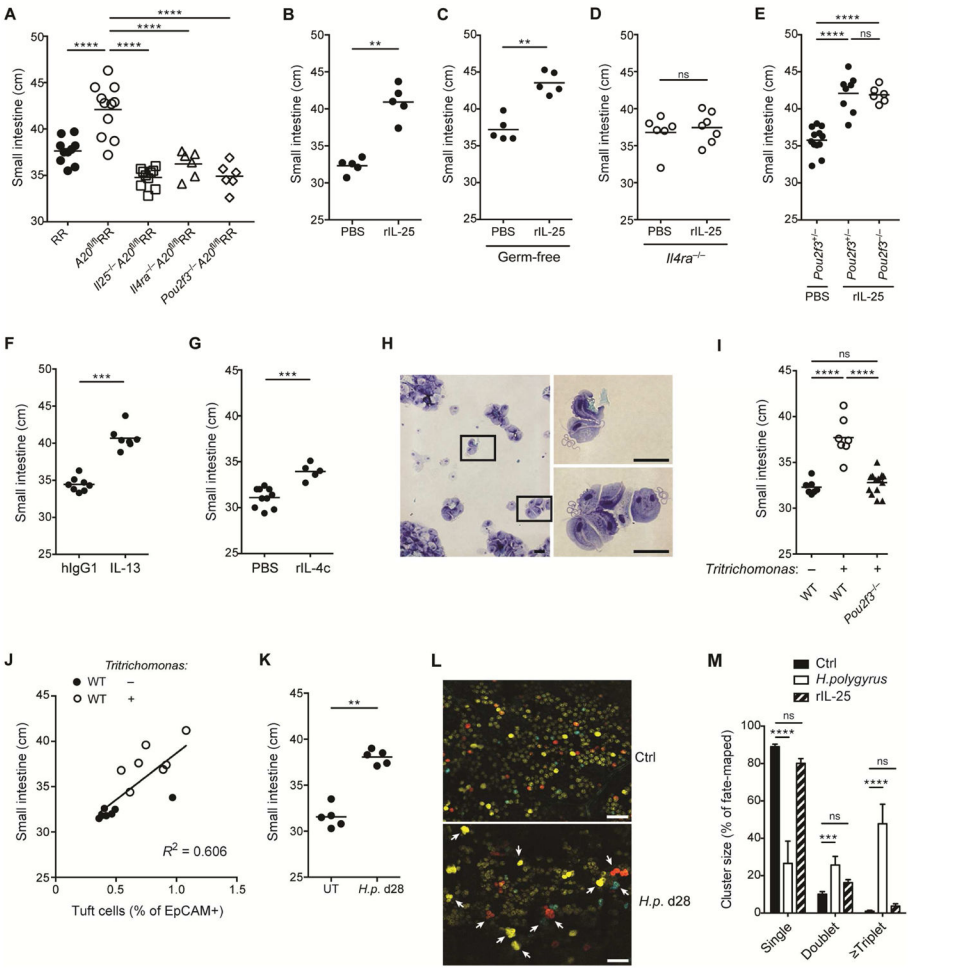

Figure 3. Activation of the tuft cell – ILC2 circuit drives small intestine lengthening

(A) Small intestine (SI) length in RR, *A20*^{fl}RR, *Il25*$^{-/-}$*A20*^{fl}RR, *Il4ra*$^{-/-}$*A20*^{fl}RR and *Pou2f3*$^{-/-}$*A20*^{fl}RR mice. (B–E) SI length in (B) wild type, (C) C57BL/6 GF, (D) *Il4ra*$^{-/-}$ and (E) *Pou2f3*$^{-/-}$ mice after 4 weeks of serial treatment with rIL-25. (F) SI length of mice 5 weeks after hydrodynamic gene delivery with IL-13 or hIgG1 control plasmid. (G) SI length of mice treated with rIL-4 complexes for 4 weeks. (H) Cytospins stained with H&E. Micrographs show representative images of *Tritrichomonas* isolated from cecum of mice housed in UCSF vivarium. Scale bars; 20 μm. (I and J) Wild type (WT) mice were colonized with purified *Tritrichomonas* at 3 weeks of age. (I) SI length measured 8 weeks later and compared to age-matched *Pou2f3*$^{-/-}$ mice naturally colonized with *Tritrichomonas*. (J) SI length of wild type mice in (I) plotted against tuft cell frequency. (K) SI length in wild type mice 28 days after infection with *H. polygyrus* (*H.p.*). (L and M) Crypt fission in the proximal SI in Lgr5-CreERT2-EGFP x R26R-Confetti mice as described in methods. (L) Representative images from mice 28 days after infection with *H. polygyrus*. Lgr5 stem cells are pseudocolored in dim yellow (Lgr5-CreERT2-EGFP) and clonal crypts are randomly marked with bright yellow (YFP), red (RFP) or blue (CFP), driven from the R26R-Confetti locus. (M) Quantification of crypt fission of mice as in (L), or after 4 weeks of serial treatment with rIL-25. Scale bars; 200 μm. Data pooled from multiple independent

experiments (A, C, D, F, M) or from one experiment representative of at least two independent experiments (B, E, G–I, L). (L, mean and s.e.m, n = 6–11). **p < 0.01, ***p < 0.001, ****p < 0.0001; ns, not significant by Mann-Whitney *U* or one-way ANOVA.

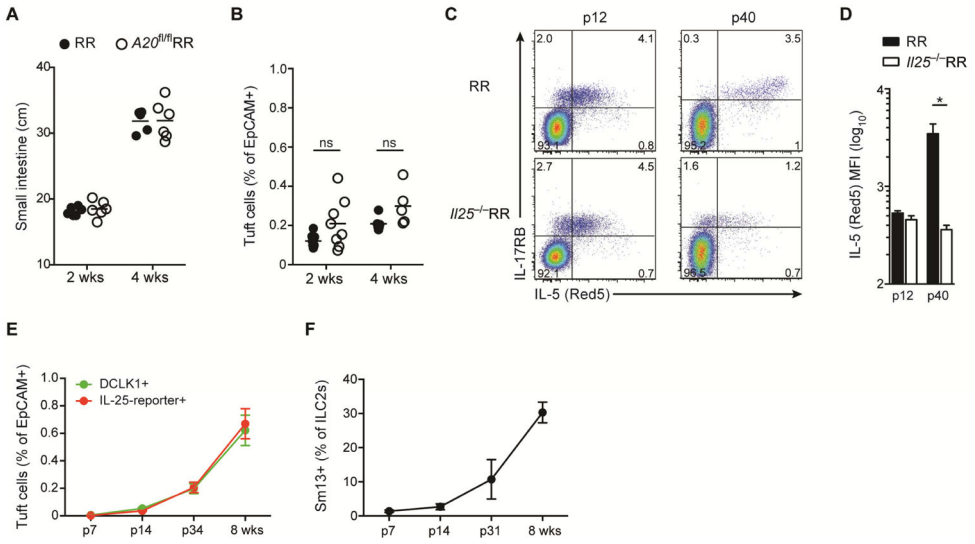

Figure 4. Weaning leads to IL-25-dependent activation of the tuft cell – ILC2 small intestinal circuit

(A and B) Small intestine (SI) length (A) and tuft cell frequencies (B) of RR and *A20*^{fl}RR mice at 2 and 4 weeks of age. (C) Expression of IL-17RB and IL-5-reporter (Red5) by cells gated on Lin- CD45+ cells isolated from SI of RR and *Il25*$^{-/-}$RR mice at days 12 and 40 post-birth (p). (D) MFI of Red5 in ILC2s gated on Lin-CD45+IL-17RB+ cells of mice as in (C). (E and F) Frequencies of tuft cells (E) based on expression of DCLK1 or IL-25-reporter and of IL-13+ (Sm13 reporter) ILC2s (F) gated on CD45+Lin-IL-17RB+ cells quantified in SI by flow cytometry at the indicated time points post-birth (p). Data pooled from multiple independent experiments (A, B, E, F) or from one experiment representative of at least two independent experiments (C and D). Student's t test was performed. (D–F, mean and s.e.m, n = 3–5). Statistical significance is indicated by *$p < 0.05$; ns, not significant.

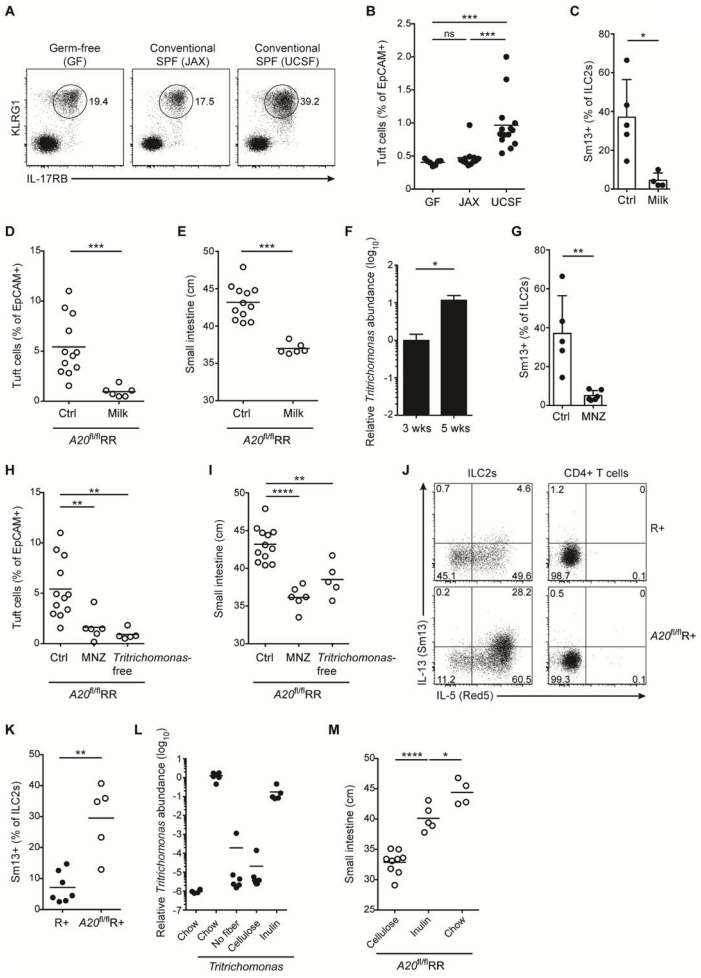

Figure 5. Dietary fibers facilitate *Tritrichomonas* colonization after weaning

(A and B) The small intestine (SI) was isolated from GF mice, or wild-type mice that were offspring of JAX mice, which were bred without further manipulation (JAX) or after colonization with *Tritrichomonas* isolated from cecal content of mice in UCSF vivarium (UCSF). Expression of KLRG1 and IL-17RB by cells gated on Lin- CD45+ cells (A) and frequencies of tuft cells (B) analyzed by flow cytometry. (C) Adult IL-13-reporter (Sm13) mice fed bovine milk as the lone dietary constituent for 2 weeks and IL-13 expression by ILC2s in SI quantified by flow cytometry. (D and E) *A20*^{fl}RR mice fed bovine milk as the lone dietary constituent following weaning for 4 weeks and frequencies of tuft cells (D) and SI length (E) were measured. (F) Abundance of *Tritrichomonas* in cecal content of WT mice at 3 and 5 weeks post-birth quantified by qPCR. (G) Adult IL-13-reporter (Sm13) mice treated with metronidazole (MNZ) in drinking water for 2 weeks and IL-13 expression by ILC2s analyzed as in (C) and compared to the same control group. (H and I) *A20*^{fl}RR mice treated with metronidazole in drinking water starting at weaning and analyzed 6–8 weeks later. *Tritrichomonas*-free *A20*^{fl}RR mice established as described in methods. The frequencies of tuft cells (H) and SI length (I) measured as in (D, E) and compared to the same control groups. (J and K) *Tritrichomonas*-free R+ and *A20*^{fl}R+ mice colonized with *Tritrichomonas* after weaning and analyzed 7 days later. Expression of IL-5 (Red5) and

IL-13 (Sm13) by ILC2s and $CD3^+CD4^+$ T cells in SI quantified by flow cytometry (J) and the frequencies of IL-13^+ ILC2s shown (K). (L) WT mice fed chow or purified diets containing no fiber, 10% cellulose or 10% inulin. One day later mice were gavaged with 10^4 purified *Tritrichomonas* and the abundance of *Tritrichomonas* in the cecum analyzed after 14 days by qPCR. (M) *A20*^{fl}RR mice fed chow or purified diets containing 10% cellulose or 10% inulin after weaning for 6 weeks and the SI length measured. Data from one experiment representative of at least two independent experiments (A, C, G, J–M) or pooled from multiple independent experiments (B, D–F, H, I). F, mean and s.e.m.; n = 5–6. *p < 0.05, **p < 0.01, ***p < 0.001, ****p < 0.0001; ns, not significant by Mann-Whitney *U* or one-way ANOVA.

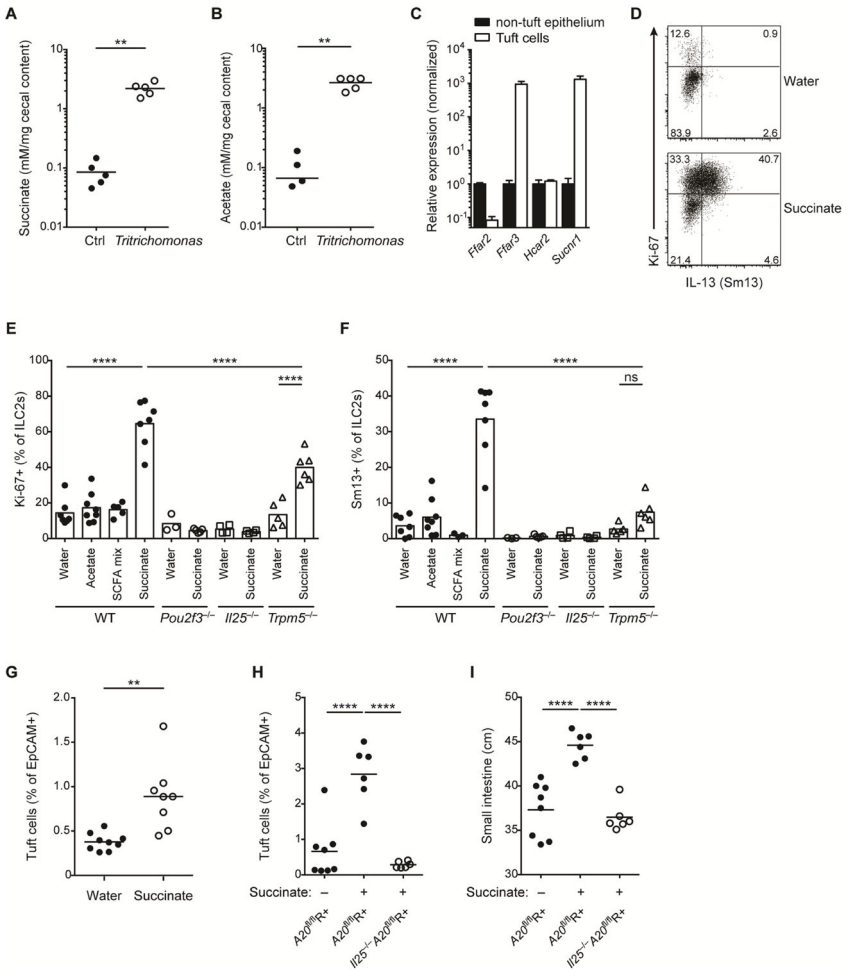

Figure 6. Succinate is produced by *Tritrichomonas* and sufficient to activate the tuft cell – ILC2 circuit

(A and B) GF mice monocolonized with *Tritrichomonas* and concentrations of acetate (A) and succinate (B) measured in the cecal content after 6 weeks. (C) Metabolite receptor mRNA expression quantified by qPCR in tuft cells versus other epithelial cells sorted from small intestine (SI) and normalized to levels in non-tuft epithelial cells. (D–F) *Tritrichomonas*-free IL-13-reporter (Sm13) mice were treated with succinate, acetate or a SCFA mix (acetate, butyrate, propionate) in drinking water for 4 days. Expression of Ki-67 and IL-13 by ILC2s in SI quantified by flow cytometry and representative dot plot from wild-type (WT) mice shown (D). Expression of Ki-67 (E) and IL-13 (F) by ILC2s from WT, *Pou2f3*$^{-/-}$, *Il25*$^{-/-}$ and *Trpm5*$^{-/-}$ *mice* treated with indicated solutions. (G) *Tritrichomonas*-free WT mice treated with 100 mM succinate in drinking water for 10 days. Frequencies of tuft cells in SI by flow cytometry. (H and I) *Tritrichomonas*-free *A20*^{fl}R+ and *Il25*$^{-/-}$*A20*^{fl}R+ mice treated with 100 mM succinate in drinking water for 25 days and frequencies of tuft cells (H) and SI length (I) analyzed. Data from one experiment (A, B) or from one experiment representative of at least two independent experiments (C, D, G–I) or pooled from multiple independent experiments (E, F). C, mean and s.e.m.; n = 3. **p < 0.01, ****p < 0.0001; ns, not significant by Mann-Whitney *U* or one-way ANOVA.

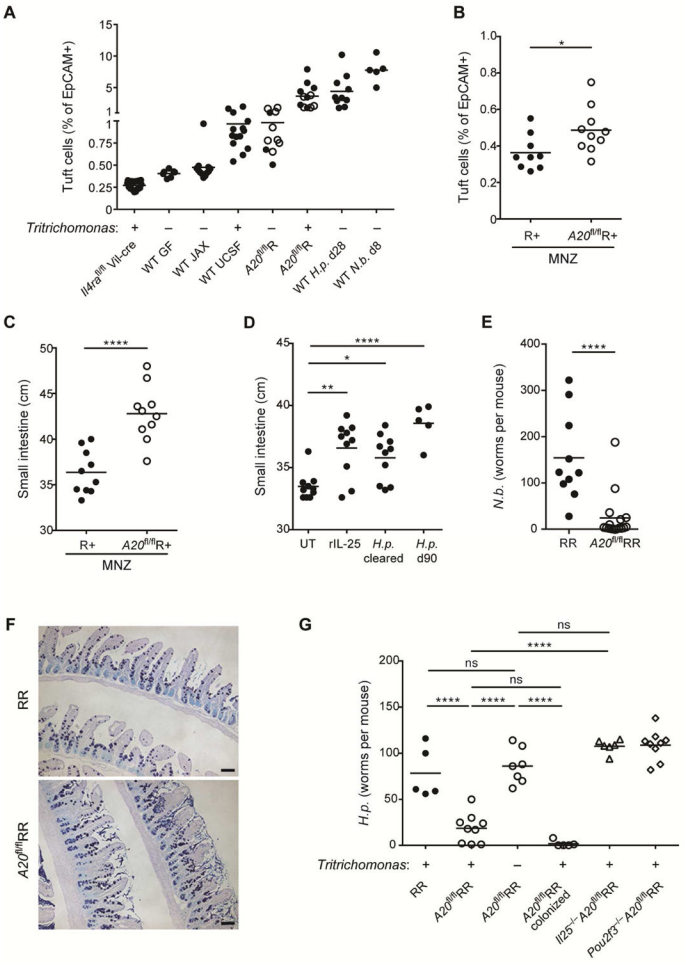

Figure 7. The tuft cell – ILC2 circuit contributes to concomitant immunity

(A) Small intestinal (SI) tuft cell frequencies in indicated mice with presence (+) or absence (−) of *Tritrichomonas* as indicated. Some data is repeated from previous figures for comparison. Wild-type (WT) mice as in Fig. 5: JAX, offsprings of mice from JAX; UCSF, offsprings of mice colonized with *Tritrichomonas*. *A20*^{fl}R pooled from *A20*^{fl}R+ (open circle) and *A20*^{fl}RR (closed circle) mice. WT mice analyzed at indicated time points after infection with *H. polygyrus* (*H.p.*) or *N. brasiliensis* (*N.b.*). (B and C) Adult R+ and *A20*^{fl}R+ mice treated with metronidazole (MNZ) in drinking water for 2 weeks and frequencies of tuft cells (B) and SI length (C) analyzed. (D) WT mice serially treated with rIL-25 or infected with *H. polygyrus* (*H.p.*) for 4 weeks followed by worm clearance (cleared) in indicated mice using pyrantel pamoate. SI length measured 2 months after the last rIL-25 administration or worm clearance. (E and F) Worm burden (E) and Alcian blue/PAS staining (F) in SI of RR and *A20*^{fl}RR mice 5 days after infection with *N. brasiliensis*. (G) SI worm counts of indicated mouse strains 13 days after infection with *H. polygyrus*. Presence (+) or absence (−) of *Tritrichomonas* indicated. One group of *Tritrichomonas*-free *A20*^{fl}RR mice was colonized with *Tritrichomonas* 2 weeks before the infection. Data pooled from multiple independent experiments (A–E) or from one experiment representative of at least two

independent experiments (F, G).*p < 0.05, **p < 0.01, ****p < 0.0001; ns, not significant by Mann-Whitney *U* or one-way ANOVA.

KEY RESOURCES TABLE

REAGENT or RESOURCE	SOURCE	IDENTIFIER
Antibodies		
Anti-mouse CD3 PB (clone 17A2)	BioLegend	Cat# 100214
Anti-mouse CD5 BV421 (clone 53-7.3)	BioLegend	Cat# 100629
Anti-mouse/human CD11b PB (clone M1/70)	BioLegend	Cat# 101224
Anti-mouse CD11c PB (clone N418)	BioLegend	Cat# 117322
Anti-mouse CD19 PB (clone 6D5)	BioLegend	Cat# 115523
Anti-mouse CD3 PE/Cy7 (clone 17A2)	BioLegend	Cat# 100220
Anti-mouse FcεRIα PB (clone MAR-1)	BioLegend	Cat# 134314
Anti-mouse TER-119 PB (clone TER-119)	BioLegend	Cat# 116232
Anti-mouse Gr-1 PB(clone RB6-8C5)	BioLegend	Cat# 108430
Anti-mouse NK-1.1 PB (clone PK136)	BioLegend	Cat# 108722
Anti-mouse CD4 BV711 (clone RM4-5)	BioLegend	Cat# 100550
Anti-mouse CD49b PB (clone DX5)	BioLegend	Cat# 108918
Anti-mouse CD8α PB (clone 53-6.7)	BioLegend	Cat# 100725
Anti-mouse TCR γ/δ BV421 (clone GL3)	BioLegend	Cat# 118120
Anti-mouse CD326 (Ep-CAM) PerCP/Cy5.5 (clone G8.8)	BioLegend	Cat# 118220
Anti-mouse F4/80 PB (clone BM8)	BioLegend	Cat# 123124
Anti-mouse CD25 BV605 (clone PC61)	BioLegend	Cat# 102036
Anti-mouse Thy1.2 BV785 (clone 30-H12)	BioLegend	Cat# 105331
Anti-mouse CD45 BUV395 (clone 30-F11)	BD Biosciences	Cat# 565967
Anti-mouse CD127 APC/eFluor780 (clone A7R34)	eBioscience	Cat# 47-1271-82
Anti-mouse KLRG1 PerCP-eF710 (clone 2F1)	eBioscience	Cat# 17-5893
Anti-mouse IL-17RB APC (clone 9B10)	BioLegend	Cat# 146308
Anti-human CD4 PE (clone RPA-T4)	eBioscience	Cat# 12-0049
Anti-human CD4 APC (clone RPA-T4)	eBioscience	Cat# 17-0049
Anti-mouse Siglec F AF647 (clone E50-2440)	BD Biosciences	Cat# 562680
Anti-mouse CD24 PE/Cy7 (clone M1/69)	BioLegend	Cat# 101822
Anti-mouse Ki-67 FITC (SolA15)	eBioscience	Cat# 11-5698-82
Anti-mouse Gata-3 PE (clone TWAJ)	eBioscience	Cat# 12-9966-42
Anti-Mouse ROR gamma (t) APC (clone B2D)	eBioscience	Cat# 17-6981-82
Anti-mouse CD3 AF488 (clone 17A2)	BioLegend	Cat# 100210
Anti-mouse ST2 PE (clone DJ8)	MD Biosciences	Cat# 101001PE
Anti-mouse ST2 Biotin (clone DJ8)	MD Biosciences	Cat# 101001B
Anti-DsRed, rabbit polyclonal	Clontech	Cat# 632496
Goat anti-Rabbit IgG (H+L)-AF555	ThermoFisher	Cat# A-21428
Anti-SP-1 Chromogranin A, rabbit polyclonal	Immunostar	Cat# 20085
Anti-Muc2, rabbit polyclonal	Santa Cruz	Cat# sc-15334
Anti-Lysozyme, rabbit polyclonal	DAKO	Cat# A009902

REAGENT or RESOURCE	SOURCE	IDENTIFIER
Anti-DCLK1, rabbit polyclonal	Abcam	Cat# ab31704
Anti-DCLK1 AF488, rabbit polyclonal	Abcam	Cat# ab203441 (custom)
Streptavidin APC	Biolegend	Cat# 405207
Goat anti-Rabbit IgG (H+L)-AF488	ThermoFisher	Cat# A-11070
Chemicals, Peptides, and Recombinant Proteins		
4′,6-Diamidine-2′-phenylindole dihydrochloride (DAPI)	Roche	Cat# 10236276001
Metronidazole	Sigma	Cat# M3761
Succinic acid	Sigma	Cat# S3674
Sodium acetate	Sigma	Cat# S2889
Recombinant Mouse IL-17E Protein, CF	R&D Systems	Cat# 1399-IL/CF
Animal-free recombinant mouse IL-4	PeproTech	Cat# AF-214-14
InVivoPlus anti-mouse IL4 antibody	Bio X Cell	Cat# BP0045
Pyrantel pamoate	Columbia Laboratories	N/A
Tamoxifen	Sigma	Cat# T5648
Critical Commercial Assays		
Succinate Assay Kit (Colorimetric)	Abcam	Cat# ab204718
Experimental Models: Organisms/Strains		
Mouse: wild-type: C57BL/6	The Jackson Laboratory	Stock# 000664
Mouse: A20^{fl}: B6.*Tnfaip3*^{tm2Ama}	Averil Ma, (Tavares et al., 2010)	N/A
Mouse: R: B6(C)-*Il5*$^{tm1.1(icre)Lky}$/J	The Jackson Laboratory	Stock# 030926
Mouse: Trpm5$^{-/-}$: B6.129P2-*Trpm5*^{tm1Dgen}/J	The Jackson Laboratory	Stock# 005848
Mouse: Lgr5EGFP-CreERT2: B6.129P2-*Lgr5*$^{tm1(cre/ERT2)Cle}$/J	The Jackson Laboratory	Stock# 008875
Mouse: R26R-Confetti: B6.129P2-*Gt(ROSA)26Sor*$^{tm1(CAG-Brainbow2.1)Cle}$/J	The Jackson Laboratory	Stock# 017492
Mouse: *Areg*$^{-/-}$: B6.*Areg*^{tm1Dle}	Marco Conti, (Luetteke et al., 1999)	N/A
Mouse: Yarg: B6.129S4-*Arg1*^{tm1Lky}/J	The Jackson Laboratory	Stock# 015857
Mouse: *Il25*$^{-/-}$: B6.*Il25*^{tm1Anjm}	Andrew N J McKenzie (Fallon et al., 2006)	N/A
Mouse: Smart13: B6.129S4(C)-*Il13*$^{tm2.1Lky}$/J	The Jackson Laboratory	Stock# 031367
Mouse: B6.YetCre-13: C.129S4(B6)-*Il13*$^{tm1(YFP/cre)Lky}$/J	The Jackson Laboratory	Stock# 017353
Mouse: B6.*Il4ra*$^{-/-}$: BALB/c-*Il4ra*^{tm1Sz}/J	The Jackson Laboratory	Stock# 003514
Mouse: IL-25 reporter	(von Moltke et al., 2016)	N/A
Mouse: B6.*Pou2f3*$^{-/-}$: C57BL/6N-*Pou2f3*$^{tm1.1(KOMP)Vlcg}$	Mark Anderson	N/A
Nippostrongylus brasiliensis	UCSF (R. Locksley)	N/A
Heligmosomoides polygyrus	UCSF (R. Locksley)	N/A
Oligonucleotides		
Rps17 (fwd) 5′-CGCCATTATCCCCAGCAAG-3′	Elim Biopharmaceuticals	N/A

REAGENT or RESOURCE	SOURCE	IDENTIFIER
Rps17 (rev) 5′-TGTCGGGATCCACCTCAATG-3′	Elim Biopharmaceuticals	N/A
A20 (fwd) 5′-ACAGGACTTTGCTACGACAC-3′	Elim Biopharmaceuticals	N/A
A20 (rev) 5′-CTGAGGATGTTGCTGAGGAC-3′	Elim Biopharmaceuticals	N/A
Il17rb (fwd) 5′-GGCTGCCTAAACCACGTAATG-3′	Elim Biopharmaceuticals	N/A
Il17rb (rev) 5′-CCCGTTGAATGAGAATCGTGT-3′	Elim Biopharmaceuticals	N/A
Tritrichomonas spp. (fwd) 5′-AGAGGAAGGAGAAGTCGTAACAAGG-3′	Elim Biopharmaceuticals	N/A
Tritrichomonas spp. (rev) 5′-CTCGTGTAAGAAGCCAAGACATCC-3′	Elim Biopharmaceuticals	N/A
Eubacteria 16S (fwd) 5′-ACTCCTACGGGAGGCAGCAGT -3′	Elim Biopharmaceuticals	N/A
Eubacteria 16S (rev) 5′-ATTACCGCGGCTGCTGGC-3′	Elim Biopharmaceuticals	N/A
Recombinant DNA		
pLIVE-hIgG1	UCSF (R. Locksley)	N/A
pLIVE-IL13	UCSF (R. Locksley)	N/A
Software and Algorithms		
FlowJo v.9.9	FlowJo	www.flowjo.com
Prism v.6.0	GraphPad	www.graphpad.com
ImageJ v.1.49	NIH	https://imagej.nih.gov/ij/
Imaris	BitPlane	http://www.bitplane.com/imaris